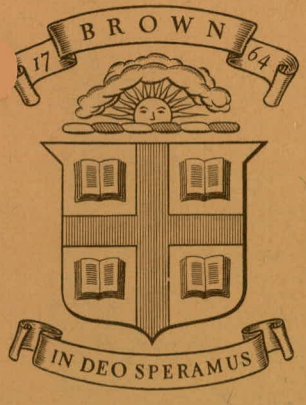

Division of Engineering
BROWN UNIVERSITY
PROVIDENCE, R. I.

CONTINUUM THEORY OF DUCTILE RUPTURE BY VOID NUCLEATION AND GROWTH: PART I - YIELD CRITERIA AND FLOW RULES FOR POROUS DUCTILE MEDIA

A. L. Gurson

U.S. Energy Research and Development Administration
Contract E(11-1)-3084
Technical Report No. 39

E (11-1)3084/39

September 1975

DISCLAIMER

Continuum Theory of Ductile Rupture by Void Nucleation and Growth: Part I - Yield Criteria and Flow Rules for Porous Ductile Media

by A. L. Gurson

Division of Engineering, Brown University, Providence, Rhode Island 02912

September 1975

Abstract

Widely used constitutive laws for engineering materials assume plastic incompressibility, and no effect on yield of the hydrostatic component of stress. However, void nucleation and growth (and thus bulk dilatancy) are commonly observed in some processes which are characterized by large local plastic flow, such as ductile fracture. The purpose of this work is to develop approximate yield criteria and flow rules for porous (dilatant) ductile materials, showing the role of hydrostatic stress in plastic yield and void growth. Other elements of a constitutive theory for porous ductile materials, such as void nucleation, plastic flow and hardening behavior, and a criterion for ductile fracture will be discussed in Part II of this series.

The yield criteria are approximated through an upper bound approach. Simplified physical models for ductile porous materials (aggregates of voids and ductile matrix) are employed, with the matrix material idealized as rigid-perfectly plastic and obeying the von Mises yield criterion. Velocity fields are developed for the matrix which conform to the macroscopic flow behavior of the bulk

material. Using a distribution of macroscopic flow fields and working through a dissipation integral, upper bounds to the macroscopic stress fields required for yield are calculated. Their locus in stress space forms the yield locus. It is shown that normality holds for this yield locus, so a flow rule results. Approximate functional forms for the yield loci are developed.

Symbols

σ_o	microscopic equivalent tensile yield stress
$\underset{\sim}{\sigma}$, σ_{ij}	microscopic stress tensor
$\underset{\sim}{s}$, s_{ij}	microscopic deviatoric stress tensor
$\dot{\underset{\sim}{\varepsilon}}$, $\dot{\varepsilon}_{ij}$	microscopic rate of deformation tensor
$\underset{\sim}{v}$, v_i	microscopic velocity field
$\underset{\sim}{x}$, x_i	microscopic position vector, cartesian coordinates
$\underset{\sim}{\Sigma}$, Σ_{ij}	macroscopic stress tensor
$\dot{\underset{\sim}{E}}$, $\dot{E}_{ij}$	macroscopic rate of deformation tensor
$\dot{\underset{\sim}{E}}'$, $\dot{E}'_{ij}$	macroscopic deviatoric rate of deformation tensor
V	volume of body
S	surface of body
$\underset{\sim}{n}$, n_i	unit normal vector on S
$\dot{W}$	macroscopic dissipation
f	void volume fraction
q_i	undefined parameters
ψ	parameter used to minimize $\dot{W}$; angle of rigid-plastic boundary
$C_1,..C_7$, $V_{32}^{\star}$, $V_{23}^{\star}$	macroscopic parameters, used to meet macroscopic boundary conditions
θ, γ	angles of rotation about the (3) axis, γ also used as an index
$\dot{E}'$, $\dot{E}$, $\dot{E}_{23}^{\star}$	macroscopic rate of deformation parameters (see eqns. 3.3)
a, b	inner and outer radius of void-matrix model
r	radius of a point inside the matrix
μ, λ	geometric parameters
Σ_{eqv}	macroscopic equivalent tensile stress
Σ_γ	macroscopic dilatational stress, cylindrical model

Σ_{kk}	macroscopic dilatational stress, spherical model
$\underset{\sim}{T}$, T_{ij}	normalized macroscopic stress
x, g	intermediate parameters
Φ	yield function
C_{eqv}	an empirical coefficient
cosh, sinh	hyperbolic cosine and sine
a_m, d_m, n_m	coefficients in arithmetic series
m	index and exponent
α	angle of rigid-plastic boundary
$\underset{\sim}{V}$, V_i	macroscopic velocity boundary conditions
$\underset{\sim}{V}^N$, V_i^N	V , normalized by b
$\mathcal{F}$	dilatation function
T_{GH}	normalized dilatation stress, cylindrical model
B_i	macroscopic yield function coefficients, functions of f
Σ_n, Σ_s	normal and shear stresses on a plane of zero extension
P, L	void radius and spacing, used in one of the references
s, v	superscripts on $\underset{\sim}{y}$ and $\dot{\underset{\sim}{\varepsilon}}$, indicating shape and volume change
r, θ, ϕ	spherical coordinates
h_{ij}	geometric parameter
Ω	solid angle
T_H	normalized dilatation stress, spherical model
δ	indicates small variation

Table of Contents

Introduction

It has been observed [1-6] that ductile fracture in metals can involve the generation of considerable porosity, via the nucleation and growth of voids. Constitutive theories which take account of porosity are therefore a desirable component of a mathematical model of the ductile fracture process. Previously developed plasticity models, such as that due to von Mises, predict plastic incompressibility and therefore could not show the dilatancy evident in porous ductile materials. In this and a companion paper (Part II), an approximate plastic constitutive theory will be developed which takes account of void nucleation and growth. This constitutive theory will then be used in a model of the ductile fracture process developed in part II.

A plastic constitutive theory can be constructed from the following components: First, a function of stress which defines the combinations of stress for which plastic yield takes place (a yield criterion) is needed. The next component is a flow rule, which defines the ratio of the strain components as a function of the stress state at yield. This can often be put in terms of the normal to the plastic potential, another function of stress. (In many cases, the yield function can be used as a plastic potential, see [7].) To relate the increment of plastic flow to the increment in stress, a consistency relation and some hardening assumptions are needed. When void nucleation as well as void growth takes place, a nucleation criterion must be added to complete the constitutive description.

In this paper, the yield criterion and flow rule for porous ductile materials are investigated. Approximate yield criteria are derived using simple rigid-plastic material models and the upper bound theorem of plasticity.

(Because void growth and ductile fracture involve large amounts of plastic flow, a rigid-plastic idealization is taken as acceptible.) A normal flow rule is established, with the approximate yield functions serving as plastic potentials. (For a discussion of the normal flow rule and its application to the specific forms of the plastic potential developed here, see the appendix.) The subjects of continuing plastic flow, hardening, void nucleation at second phases, and predictions of ductility (strain to fracture) will be investigated in the subsequent paper.

Along with the observations cited above, some recent theoretical studies [8-10] indicate that when voids are present in ductile materials, the hydrostatic component of stress can cause macroscopic dilatation and affect plastic yield. Because the material surrounding the void is idealized as incompressible, the dilatation is due completely to void growth. The approximate yield functions (usable as plastic potentials) developed here will contain terms which are functions of hydrostatic stress, and thus allow plastic dilatancy through the normality rule.

The general physical model used here is a "unit" cube not unlike that of Bishop and Hill [11], only of a porous material (aggregate of voids and ductile matrix) rather than a polycrystalline aggregate. The cube is by definition large enough to be statistically representative of the properties of the aggregate. As Berg [12] has pointed out, the Bishop and Hill analysis can be extended to apply to a porous material. This allows proof of a macroscopic maximum plastic work principle for the aggregate, if the same principle applies locally to the matrix material. Throughout this paper, the adjective "macroscopic" refers to average values of physical quantities (stress, dissipation, velocity, etc.) which represent the aggregate behavior.

"Microscopic" refers to pointwise quantities, such as the stress or velocity fields in the ductile matrix.

The general method used here to calculate an upper bound yield function for a void-matrix aggregate is as follows: The von Mises equations are used to characterize the yield and flow behavior of the matrix, which is itself incompressible. An approximate form is then assumed for the microscopic velocity field in the matrix, which allows the voids to change volume while maintaining matrix incompressibility. This velocity field must obey compatibility, and meet kinematic boundary conditions on the surface of the unit cube which correspond to prescribed macroscopic rates of deformation. An upper bound inequality is then used to calculate upper bounds to the macroscopic stresses required to sustain plastic flow. The locus of upper bound macroscopic stresses for a given void geometry (size, shape, distribution, etc.) and a range of macroscopic rate of deformation fields form an upper bound yield locus for that unit cube. Given certain restrictions on the approximate microscopic velocity field, a maximum plastic work principle can be established for the upper bound yield locus. (Bishop and Hill establish one for the true yield locus). A functional form which gives a good fit to the upper bound yield locus can be called the approximate (upper bound) yield function.

For purposes of analysis, the void-matrix aggregate is idealized as a single void in a rigid-plastic cell; the void volume fraction (f) of the cell equalling that of the aggregate. (In this way, some account is taken of the interaction of neighboring voids). The cell is presumed to behave under loading as the aggregate would, exhibiting void growth when undergoing yield with a positive hydrostatic component of macroscopic stress. Two void geometries are con-

dered; the long circular cylinder and the sphere. The outer cell wall is

idealized as geometrically similar to, and centered around the void. These geometries were chosen because they resemble many of the void shapes seen experimentally, they provide the expected isotropy (transverse directions for the cylinder, total for the sphere), and because their symmetry properties significantly aid the analysis. See figs. 1, 2, and 3.

These simple cell models will not, of course behave exactly like aggregates with random distributions of voids. Therefore, the upper bound yield loci obtained for the cell models are in a strict sense only estimates (bounding properties unknown) of the yield loci for more random aggregates.

The approximate velocity fields used in the upper bound calculations can be simple or complex, depending on the degree of approximation desired. The simplest fields need only meet those conditions discussed previously. More complex fields may contain extra factors which can be adjusted to achieve better upper bounds. The simplest velocity fields allow the rigorous determination of functional forms for the upper bound yield functions, thus giving a clear (if approximate) picture of the role of hydrostatic stress in the yield and flow of porous ductile materials.

Some of the previous work done in this field is as follows: McClintock [8] developed a fracture criterion based on his analysis of a cylindrical cavity in an infinite matrix subject to axial and transverse stresses. An exponential dependence of the void growth rate on biaxial stress was found. Rice and Tracey [9] considered a spherical void in an infinite matrix, and found an exponential dependence of void growth rate on triaxial stress. Kahlow and Avitzur [10] studied the problem of the critical pressure needed to prevent void growth during axially symmetric deformation. Their model was a closed

cylinder of ductile material with a cylindrical hole at the center, and their approach was in some ways similar to that used here.

There are several studies which motivated the examination of more complex microscopic flow fields. Nagpal, McClintock, Berg, and Subudhi [13] presented a plane strain slip line solution for a band of evenly spaced holes under varying ratios of shear and normal traction. Needleman [14], and Haward and Owen [15] presented finite element studies of large flow in two-dimensional models of porous materials, using elastic-plastic constitutive descriptions for the matrix material. Specifically, these studies suggest that part of the matrix might not attain plastic yield for some types of aggregate yield. These "non-plastic" areas are idealized as rigid here. Their shapes are approximated as shown in fig. 4.

2. General Theory

The general model considered here is a "unit" cube of porous material of volume V, large enough to be statistically representative of the properties of the aggregate (Fig. 1). The matrix material is a homogeneous, incompressible, rigid-plastic, von Mises material. Its yield and flow relations are

$$\frac{3}{2} s_{ij}s_{ij} = \sigma_o^2 \quad (a) , \qquad s_{ij}(\dot{\underset{\sim}{\varepsilon}}) = \frac{\sqrt{\frac{2}{3}}\sigma_o \dot{\varepsilon}_{ij}}{(\dot{\varepsilon}_{k\ell}\dot{\varepsilon}_{k\ell})^{1/2}} \quad (b)$$

$$\dot{\varepsilon}_{ij} = \frac{1}{2}\left(\frac{\partial v_i}{\partial x_j} + \frac{\partial v_j}{\partial x_i}\right) , \qquad \dot{\varepsilon}_{kk} = 0 \quad (c) \tag{2.1}$$

where σ_o is the equivalent tensile yield stress in the matrix, s_{ij} the microscopic deviatoric stress field, $\dot{\varepsilon}_{ij}$ is the microscopic rate of deformation field, v_i is the microscopic velocity field, and x_i is the position of a material point in cartesian coordinates.

The macroscopic rate of deformation is defined, as in Bishop and Hill [11], in terms of the velocity field on the surface of the unit cube.

$$\dot{E}_{ij} = \frac{1}{V}\frac{1}{2}\int_S (v_i n_j + v_j n_i) dS \ . \tag{2.2}$$

V is the volume of the unit cube, S is its outer surface, and $\underset{\sim}{n}$ is the unit outward normal on S. Using the Gauss theorem and eqn. 2.1c, it can be shown that

$$\dot{E}_{ij} = \frac{1}{V}\int_V \dot{\varepsilon}_{ij} dV \ . \tag{2.3}$$

Where $\underset{\sim}{n}$ is still a surface normal in the outward direction, this can be separated into integrals over the matrix material and the void surface:

$$\dot{E}_{ij} = \frac{1}{V}\int_{V_{matrix}} \dot{\varepsilon}_{ij} dV + \frac{1}{V}\frac{1}{2}\int_{S_{voids}} (v_i n_j + v_j n_i) dS \ . \tag{2.4}$$

The last term above includes the dilatational part of $\dot{E}_{ij}$, and is zero when there is no porosity. The boundary conditions on the outer surface which must be met by the v_i field are expressed in terms of the $\dot{E}_{ij}$. It is important to note the $\dot{E}_{ij}$ are average quantities (eqn. 2.2), and can represent many different boundary distributions of v_i .

The velocity field must also meet the constraints of incompressibility and continuity in the matrix. Velocity fields which involve matrix separation are therefore excluded.

Among the infinity of incompressible v_i fields which meet the above conditions, the actual v_i field is characterized by its generation of the minimum of the dissipaiton $\dot{W}$;

$$\dot{W} = \frac{1}{V}\int_V s_{ij}(\dot{\underset{\sim}{\varepsilon}})\dot{\varepsilon}_{ij}\,dV \qquad (2.5)$$

where the terms in the integrand are related to v_i by eqns. 2.1. (This is proven later on; see eqn. 2.23.) All physical quantities associated with the actual v_i field will be labeled with the superscript "A", since they are also actual solutions. Quantities associated with other v_i fields are approximate solutions. An important property of σ^A_{ij} is that it is an equilibrium stress field. It is expected that v^A_i is homogeneous of degree one in the $\dot{E}_{ij}$.

Bishop and Hill postulate that no correlation exists between σ^A_{ij} and position or displacement (velocity) over any plane section through the unit cube. They also establish a maximum plastic work principle on the microscopic level, which also applies to $s_{ij}(\dot{\underset{\sim}{\varepsilon}})$ as defined in eqn. 2.1:

$$\left[s_{ij}(\dot{\underset{\sim}{\varepsilon}}) - s_{ij}(\dot{\underset{\sim}{\varepsilon}}^*)\right]\dot{\varepsilon}_{ij} \geq 0 \quad , \quad \dot{\underset{\sim}{\varepsilon}} \neq \dot{\underset{\sim}{\varepsilon}}^* \; . \qquad (2.6)$$

Using the non-correlation postulate (above) and the principle of virtual work, Bishop and Hill are able to prove that, when Σ^A_{ij} is defined as the area average of σ^A_{ij} over the appropriate face of the unit cube, $\underset{\sim}{\Sigma}^A$ is the work conjugate of $\dot{\underset{\sim}{E}}$:

$$\Sigma^A_{ij} = \frac{1}{A}\int_A \sigma^A_{ij}\,dS \rightarrow \dot{W}^A = \Sigma^A_{ij}\dot{E}_{ij} \quad . \tag{2.7}$$

Using the principle of virtual work, they are then able to prove a maximum plastic work principle on the macroscale for $\underset{\sim}{\Sigma}^A$:

$$(\Sigma^A_{ij} - \Sigma^{A*}_{ij})\dot{E}_{ij} \geq 0 \quad , \tag{2.8}$$

where $\underset{\sim}{\Sigma}^{A*}$ is related to $\dot{\underset{\sim}{E}}^*$, and $\dot{\underset{\sim}{E}}^*$ differs from $\dot{\underset{\sim}{E}}$. The yield locus of $\underset{\sim}{\Sigma}^A$ thus has the properties of convexity and normality. Equations 2.7 and 2.8 can then be combined to show

$$\delta W^A = \delta\Sigma^A_{ij}\dot{E}_{ij} + \Sigma^A_{ij}\delta\dot{E}_{ij} \quad ,$$

$$\delta\Sigma^A_{ij}\dot{E}_{ij} = 0 \quad \text{by normality}$$

$$\therefore \quad \Sigma^A_{ij} = \frac{\partial\dot{W}^A}{\partial\dot{E}_{ij}} \quad . \tag{2.9}$$

$\dot{\varepsilon}^A_{ij}$ was derived from v^A_i , the actual velocity field, and gave the actual dissipation through eqn. 2.5. When an approximate field v_i is used, eqn. 2.5 defines an approximate dissipation. The v_i fields considered here have the functional form

$$v_i = v_i(\dot{\underset{\sim}{E}}, f, \underset{\sim}{x}) \quad . \tag{2.10}$$

There may be additional dependence on other parameters q_1 , q_2 , ... , as in

$$v_i = v_i(\dot{\underset{\sim}{E}}, f, \underset{\sim}{x}, q_1, q_2 \ldots) \tag{2.11}$$

with the q_i's chosen to minimize the dissipation. For these optimal values,

$$q_i = q_1(\dot{\underset{\sim}{E}}, f) \tag{2.12}$$

so the form of eqn. 2.11 reduces to that of eqn. 2.10. All of the forms of v_i considered here are homogeneous of degree one in the components of $\dot{\underset{\sim}{E}}$, i.e.,

$$\text{for } c = \text{constant}, \quad v_i(c\dot{E}_{11}, c\dot{E}_{22}, \ldots) = cv_i(\dot{E}_{ii}, \dot{E}_{22}, \ldots) \tag{2.13}$$

$\dot{\underset{\sim}{\varepsilon}}$ and $\dot{W}$ are then also homogeneous of degree one in the $\dot{E}_{ij}$, giving

$$\dot{W} = \frac{\partial \dot{W}}{\partial \dot{E}_{ij}} \dot{E}_{ij} \quad . \tag{2.14}$$

Define the approximate macroscopic stress needed to cause yielding (via the flow field v_i) in a way analogous to eqn. 2.9:

$$\Sigma_{ij} = \frac{\partial \dot{W}}{\partial \dot{E}_{ij}} = \frac{1}{V} \int_V s_{k\ell}(\dot{\underset{\sim}{\varepsilon}}) \frac{\partial \dot{\varepsilon}_{k\ell}}{\partial \dot{E}_{ij}} \, dV \quad , \tag{2.15}$$

using the normality of $s_{ij}(\dot{\underset{\sim}{\varepsilon}})$ (see eqn. 2.6) to set one part of the integrand to zero. This gives, with eqn. 2.14

$$\Sigma_{ij}\dot{E}_{ij} = \frac{\partial \dot{W}}{\partial \dot{E}_{ij}} \dot{E}_{ij} = \dot{W} \quad . \tag{2.16}$$

Thus, Σ_{ij} as defined above is a work conjugate to $\dot{E}_{ij}$, as is Σ^A_{ij}. By analogy with eqn. 2.9, normality is thus established for the approximate yield locus (the locus of stress states Σ_{ij} defined by eqn. 2.15, for all possible directions of $\dot{E}_{ij}$).

A maximum plastic work principle has been established for $\underset{\sim}{\Sigma}^A$, giving both convexity and normality. It is desirable to examine under what conditions this might also be established for $\underset{\sim}{\Sigma}$. Consider two approximate stress fields $\underset{\sim}{\Sigma}$ and $\underset{\sim}{\Sigma}^*$, corresponding to $\dot{\underset{\sim}{E}}$ and $\dot{\underset{\sim}{E}}^*$ respectively through eqns. 2.15, 2.10, 2.2, and

1. Write the following:

$$(\Sigma_{ij}-\Sigma^{*}_{ij})E_{ij} = \frac{1}{V}\int_V \left\{ s_{k\ell}(\dot{\underset{\sim}{\varepsilon}})\frac{\partial \dot{\varepsilon}_{k\ell}}{\partial \dot{E}_{ij}} - s_{k\ell}(\dot{\underset{\sim}{\varepsilon}}^{*})\frac{\partial \dot{\varepsilon}^{*}_{k\ell}}{\partial \dot{E}^{*}_{ij}} \right\} \dot{E}_{ij}\, dV \quad . \tag{2.17}$$

If this could be proven non-negative, a maximum plastic work principle would result. Consider the case of $\dot{\underset{\sim}{\varepsilon}}$ not only homogeneous of degree one, but <u>linear</u> in $\dot{\underset{\sim}{E}}$. Then,

$$\frac{\partial \dot{\varepsilon}^{*}_{k\ell}}{\partial \dot{E}^{*}_{ij}}\dot{E}_{ij} = \frac{\partial \dot{\varepsilon}_{k\ell}}{\partial \dot{E}_{ij}}\dot{E}_{ij} = \dot{\varepsilon}_{k\ell} \quad . \tag{2.18}$$

With maximum plastic work proven on the microscopic level, the proof is complete.

Equation 2.18 applies to one class of velocity fields used later on. A second class, to which it does not apply, is of the form

$$v_i = v_i(\dot{\underset{\sim}{E}}, f, \underset{\sim}{x}, \psi) \tag{2.19}$$

where v_i, and thus $\dot{\underset{\sim}{\varepsilon}}$ and $\dot{W}$, are homogeneous and linear in the $\dot{E}_{ij}$ for a fixed value of ψ. ψ is an additional parameter equivalent to q_i in eqn. 2.12, and has the effect of making v_i homogeneous of degree one, but no longer linear, in the $\dot{E}_{ij}$. The approximate dissipation thus has the form

$$\dot{W} = \dot{W}\left(\dot{\underset{\sim}{E}}, f, \psi(\dot{\underset{\sim}{E}}, f)\right) \quad . \tag{2.20}$$

Equation 2.15 gives

$$\Sigma_{ij} = \left.\frac{\partial \dot{W}}{\partial \dot{E}_{ij}}\right|_{\psi=\text{const}} + \left.\frac{\partial \dot{W}}{\partial \psi}\right|_{E=\text{const}} \cdot \frac{\partial \psi}{\partial \dot{E}_{ij}} \quad . \quad \text{(a)} \tag{2.21}$$

Because $\psi(\dot{\underset{\sim}{E}}, f)$ is determined by minimizing $\dot{W}$ with respect to ψ,

$$\frac{\partial \dot{W}}{\partial \psi} = 0 \quad . \quad \text{(b)} \tag{2.21}$$

Unfortunately, the dependence of ψ on $\dot{\underset{\sim}{E}}$ makes it impossible to prove convexity from eqn. 2.17. Convexity can be used, however, to help judge the value of

approximate yield functions generated with this formulation. Since the object is to approximate the actual yield and flow behavior, an approximation which violates convexity should be considered a bad approximation.

To prove that the approximate yield locus lies outside the actual yield locus in stress space, write the principle of maximum plastic work in the following form:

$$\frac{1}{V}\int_V \left(s_{ij}(\dot{\underset{\sim}{\varepsilon}}) - s_{ij}(\dot{\underset{\sim}{\varepsilon}}^A)\right)\dot{\varepsilon}_{ij}\,dV \geq 0 \quad , \tag{2.22}$$

where the s_{ij} are of the form in eqn. 2.1, and both $\dot{\underset{\sim}{\varepsilon}}$ and $\dot{\underset{\sim}{\varepsilon}}^A$ are compatible with the same macroscopic rate of deformation $\dot{\underset{\sim}{E}}$. Using eqn. 2.5, the principle of virtual work, and the result that both $\underset{\sim}{\Sigma}$ and $\underset{\sim}{\Sigma}^A$ are work conjugates to $\underset{\sim}{E}$, eqn. 2.22 becomes

$$(\Sigma_{ij} - \Sigma^A_{ij})\,\dot{E}_{ij} \geq 0 \quad . \tag{2.23}$$

Since $\dot{E}_{ij}$ is an outward normal to both the Σ_{ij} and Σ^A_{ij} yield loci, this proves that the Σ_{ij} surface always lies on or outside the Σ^A_{ij} surface; $\underset{\sim}{\Sigma}$ is an upper bound approximation to $\underset{\sim}{\Sigma}^A$.

The most important properties established for the approximate macroscopic yield stress are its upper bound relationship to $\underset{\sim}{\Sigma}^A$, the normality and convexity (given the conditions described above) properties of its yield locus, and eqns. 2.15 and 2.21 which give its relationship to $\dot{\underset{\sim}{E}}$. Subsequent sections of this paper are devoted to the solution of eqns. 2.15 and 2.21 for various types of v_i fields, ranges of $\dot{\underset{\sim}{E}}$, ranges of void volume fraction f, and the two void geometries discussed earlier. Varying the $\dot{\underset{\sim}{E}}$ field results in the generation of an approximate yield locus for a particular void geometry, volume fraction, and flow field type. With some success, approximate functional forms are derived for these yield loci.

3a. Long Circular Cylindrical Voids - Fully Plastic Flow

This void geometry is meant to represent one limit of random void shape. Long, roughly cylindrical voids are seen to appear at the necks of tensile bars after large deformation (see, for example, ref. [3]). They might also result from long cylindrical inclusions (e.g., sulfides in steels) which decohere from the matrix after straining, or on a larger scale, from drilled holes in a homogeneous material. The centered and geometrically similar matrix displays the transverse isotropy expected of an aggregate with an isotropic matrix and a void distribution which is random in the transverse directions.

For the type of flow field considered here, in which all of the matrix material is in the plastic state, a simplified form of eqn. 2.2 is used as the boundary conditions on v_i :

$$v_i|_S = \dot{E}_{ik} x_k|_S \quad \text{(cartesian coordinates)} \tag{3.1}$$

The boundary values of v_i are thus uniquely defined by the $\dot{E}_{ij}$. In other formulations, the boundary distribution of v_i will be varied, within the constraints of eqn. 2.2 and certain geometric approximations to achieve the best upper bound solution.

The approximate velocity field is constructed in a manner similar to that used by Rice and Tracey [9]; components representing shear and dilatation are constructed separately, each satisfying compatibility and incompressibility. These components are determined to within macroscopic parameters, which are in turn determined by boundary conditions of the form of eqn. 3.1. When the form

of a component is not completely determinable from symmetry and incompressibility, a general form is constructed in accord with a linear viscous (or equivalently, an incompressible elastic) model. This approach leads to more macroscopic parameters than can be determined from boundary conditions alone, so other conditions, leading to refined velocity fields and lower values of $\dot{W}$, are devised. This calculation is carried out in ref. [17], and draws on an example in ref. [16].

The general results are as follows:

$$v_r = (C_1 r^3 + C_2 r + C_3 r^{-1} + C_4 r^{-3}) \cos 2\theta + V_{32}^{\star} z \cos\gamma + \frac{C_7}{r} - \dot{E}_{33}\frac{r}{2} \qquad (3.2)$$

$$v_\theta = (-2C_1 r^3 - C_2 r + C_4 r^{-3}) \sin 2\theta - V_{32}^{\star} z \sin\gamma, \quad v_z = \dot{E}_{33} z + (C_5 r + C_6 r^{-1}) \cos\gamma$$

C_1 through C_7 and V_{32} are the macroscopic parameters referred to above. The angle θ is referred to transverse axes in which $\dot{E}_{12}$ is zero, and the angle γ is referred to axes in which $\dot{E}_{13}$ is zero. (This is done to facilitate the application of boundary conditions - again, the details are in ref. [17]). $V_{32}^{\star}$ is the shearing velocity per unit axial length. In fig. 2, the axes are such that $\dot{E}_{12} = 0$. Quantities in the axes where $\dot{E}_{13} = 0$ (reached by a rotation about the (3) axis) are denoted by the superscript "$\star$".

Boundary conditions are applied at the outer boundary ($r = b$) in terms of the new macroscopic variables defined below. $V_{23}^{\star}$ is a normalized shear velocity parallel to the (3) axis, and is in the same spirit at $V_{32}^{\star}$(eqn.3.2).

$$\dot{E}' \equiv \frac{1}{2}(\dot{E}_{22} - \dot{E}_{11}) \text{ (a)}, \quad \dot{E} \equiv \frac{1}{2}\dot{E}_{kk} \equiv \frac{1}{2}(\dot{E}_{11} + \dot{E}_{22} + \dot{E}_{33}) \text{ (b)}, \quad \dot{E}_{23}^{\star} = E_{32}^{\star} \equiv \frac{1}{2}(V_{23}^{\star} + V_{32}^{\star}) \text{ (c)} \qquad (3.3)$$

The velocity field on the outer surface is, in terms of these macroscopic quantities;

$$v_r|_S = \dot{E}'b\cos(2\theta) + \frac{1}{2}(\dot{E}_{22} + \dot{E}_{11})\,b + V^{\star}_{32}\cdot z\cdot\cos(\gamma),$$

$$v_z|_S = V^{\star}_{23}b\cos(\gamma) + \dot{E}_{33}\cdot z,\quad v_\theta|_S = -\dot{E}'b\sin(2\theta) - V^{\star}_{32}\sin(\gamma) \qquad (3.4)$$

These are three equations in the seven unknowns C_1 through C_7. Some methods for determining the four additional equations needed for a solution are discussed below.

First, consider setting C_1 equal to zero. C_1 approaches zero when f is very small in the previously cited elastic example [16]. Also, it seems reasonable that $\underset{\sim}{v}$ should approach linearity in r for r>>a ('a' is the void radius). This can be true only if C_1 is zero. For these reasons, the approximation

$$C_1 = 0 \qquad (3.5)$$

is adopted.

It is reasonable to expect that a good approximate flow field will behave in a manner closely resembling the actual flow field. Note now that the void surface is free of both normal and shear tractions. Because the matrix is a von Mises material, the related shear deformation rates are also zero at the void surface (see eqn. 2.1b)

$$\dot{\varepsilon}_{r\theta}|_{r=a} = \dot{\varepsilon}_{rz}|_{r=a} = 0 \qquad (3.6)$$

(Of course, an equivalent statement for normal components of traction and $\underset{\sim}{\dot{\varepsilon}}$ does not apply.)

A fourth and final condition results from minimizing the macroscopic dissipation, $\dot{W}$. These procedures are carried out in detail in ref. [17]. Equations

3.4, 3.5, and 3.6 are used to reduce the number of undetermined C_i to one. This last value is determined by finding its value which minimizes $\dot{W}$.

The details of this calculation are omitted here. The results have a functional form very close to the result of a much simpler calculation, which is described below.

Suppose that in addition to C_1, the coefficients C_3, C_4, and C_6 are also set to zero. Then,

$$v_r = C_2 r \cos(2\theta) + \frac{C_7}{r} - \dot{E}_{33}\frac{r}{2} + V_{32}^{\star} z \cos(\gamma),$$

$$v_\theta = -C_2 r \sin(2\theta) - V_{32}^{\star} z \sin(\gamma), \quad v_z = \dot{E}_{33} \cdot z + C_5 r \cos(\gamma) . \tag{3.7}$$

Equating v at $r = b$ with the boundary conditions in eqn. 3.4 gives

$$C_2 = \dot{E}', \; C_5 = V_{23}^{\star}, \text{ and } C_7 = \frac{1}{2}\dot{E}_{kk} b^2 ,$$

$$\dot{\varepsilon}_{rr} = \dot{E}' \cos(2\theta) - \dot{E} b^2 r^{-2} - \frac{1}{2}\dot{E}_{33}, \; \dot{\varepsilon}_{\theta\theta} = -\dot{E}' \cos(2\theta) + \dot{E} b^2 r^{-2} - \frac{1}{2}\dot{E}_{33}, \tag{3.8}$$

$$\dot{\varepsilon}_{zz} = \dot{E}_{33}, \; \dot{\varepsilon}_{r\theta} = -\dot{E}' \sin(2\theta), \; \dot{\varepsilon}_{rz} = \frac{1}{2}(V_{23}^{\star} + V_{32}^{\star}) \cos(\gamma),$$

$$\dot{\varepsilon}_{\theta z} = -\frac{1}{2}(V_{23}^{\star} + V_{32}^{\star}) \sin(\gamma), \equiv -\dot{E}_{23}^{\star} \sin(\gamma) .$$

Equations 3.8 describe an approximate $\dot{\underset{\sim}{\varepsilon}}$ field in which the deviatoric part has been set equal to the deviatoric part of $\dot{\underset{\sim}{E}}$, and a dilatational part added on which is derived from $\dot{E}_{kk}$, $\dot{E}_{33}$, and matrix incompressibility. This $\dot{\underset{\sim}{\varepsilon}}$ field will now be used to solve for $\underset{\sim}{\Sigma}$ via eqn. 2.15.

The dissipation can be written as follows, using eqns. 2.5 and 2.1

$$\dot{W} = \frac{1}{V}\int_V \sqrt{\frac{2}{3}}\,\sigma_o \cdot (\dot{\varepsilon}_{ij}\dot{\varepsilon}_{ij})^{1/2}\, dV . \tag{3.9}$$

Using eqns. 3.8, and referring all quantities to the same axes;

$$\dot{\varepsilon}_{ij}\dot{\varepsilon}_{ij} = 2\dot{E}'^2 + \dot{E}_{12}^2 + \dot{E}_{21}^2 + 4\mu\dot{E}'\dot{E}_\lambda^{-1} + 2\dot{E}^2\lambda^{-2} + \frac{3}{2}\dot{E}_{33}^2 + \dot{E}_{13}^2 + \dot{E}_{31}^2 + \dot{E}_{23}^2 + \dot{E}_{32}^2 \quad (a) \tag{3.10}$$

where

$(\dot{E}_{23}^{\star})^2 = \dot{E}_{13}^2 + \dot{E}_{23}^2$ (b), $\mu = \cos(2\theta)$, θ measured c.c.w. from (2) axis (c), $\lambda \equiv \frac{r^2}{b^2}$ (d)

It is assumed that σ_o is constant in the matrix when eqn. 2.15 is applied.

The locus of $\underset{\sim}{\Sigma}$ in stress space which is related to the entire range of $\dot{\underset{\sim}{E}}$ (the yield locus) will be expressed approximately in terms of the macroscopic equivalent tensile stress, and the macroscopic transverse stress:

$$\Sigma_{eqv}^2 = \left(\frac{3}{2}\Sigma'_{ij}\Sigma'_{ij}\right), = \frac{3}{4}(\Sigma_{22}-\Sigma_{11})^2 + \frac{9}{4}\Sigma_{33}'^2 + \frac{3}{2}(\Sigma_{12}^2+\Sigma_{21}^2) + \frac{3}{2}(\Sigma_{\gamma 3}\Sigma_{\gamma 3}+\Sigma_{3\gamma}\Sigma_{3\gamma}),$$

$$\gamma = 1,2 \text{ and } \Sigma_{\gamma\gamma}, = \Sigma_{11} + \Sigma_{22} \tag{3.11}$$

Note that summation over a Greek index is over one and two.

The stress components in eqn.3.11, when calculated via eqn. 2.15, are expressed as volume integrals which contain the components of $\dot{\underset{\sim}{E}}$ and the angular and radial terms μ and λ. The general method of solution (described in ref. [17]) was to expand the integrands into polynomials in μ, integrate over μ, and then perform the radial integration. It was found that for this simple flow field (eqn. 3.8) the relation between Σ_{eqv} and $\Sigma_{\gamma\gamma}$ was invariant to $\dot{\underset{\sim}{E}}$, to within first order in μ. Numerical integration of several specific cases showed that the approximation was a good one. The analysis is outlined below for the simplest case; axisymmetric deformation.

Because σ_o is a constant, use the following normalization:

$$\underset{\sim}{T} = \frac{\underset{\sim}{\Sigma}}{\sigma_o} \quad . \tag{3.12}$$

Due to axial symmetry, the stress system is

$$T_{11} = T_{22} \; , \; T_{eqv} = |T_{33} - T_{11}| \; , \; T_{\gamma\gamma} = 2T_{11} \; . \tag{3.13}$$

Using eqn. 2.15,

$$T_{33} - T_{11} = \frac{\sqrt{3}}{2}\frac{1}{V}\int_V \dot{E}_{33}(\dot{E}^2\lambda^{-2} + \frac{3}{4}\dot{E}_{33}^2)^{-1/2}dV, T_{\gamma\gamma} = \frac{2}{\sqrt{3}}\frac{1}{V}\int_V \dot{E}\lambda^{-2}(\dot{E}^2\lambda^{-2} + \frac{3}{4}\dot{E}_{33}^2)^{-1/2}dV \tag{3.14}$$

The following changes of variable are used:

$$\frac{1}{V}\int_V dV = \frac{1}{\pi b^2 L}\int_0^L\int_0^{2\pi}\int_a^b dr\, d\theta\, dz, = \int_f^1 d\lambda \text{ for axial symmetry}$$

$$x \equiv E\lambda^{-1}, \; g \equiv \frac{3}{4}\dot{E}_{33}^2 \tag{3.15}$$

Equations 3.14 can now be written

$$T_{eqv} = g^{1/2}\,\dot{E}\int_{\dot{E}}^{\dot{E}/f} x^{-2}(x^2+g)^{-1/2}dx, \; T_{\gamma\gamma} = \frac{2}{\sqrt{3}}\int_{\dot{E}}^{\dot{E}/f}(x^2+g)^{-1/2}dx$$

These integrals can be found in many standard reference tables (e.g., ref. [21]). The results are

$$T_{II}, \equiv g^{1/2}T_{eqv} = (\sqrt{\dot{E}^2+g} - \sqrt{\dot{E}^2+gf^2}), T_I, \equiv \frac{\sqrt{3}}{2}T_{\gamma\gamma} = \ell n\left\{\frac{\sqrt{\dot{E}^2+gf^2} + \dot{E}}{f(\sqrt{\dot{E}^2+g} + \dot{E})}\right\} \tag{3.17}$$

$\dot{E}$ and g can be eliminated between eqns. 3.17 to give an equation in T_{eqv}, $T_{\gamma\gamma}$, and f, which is the approximate yield function ([22],[17]).

The result is

$$\Phi = T_{eqv}^2 + 2f \cosh\left(\frac{\sqrt{3}}{2} T_{\gamma\gamma}\right) - 1 - f^2 = 0 \tag{3.18}$$

which is the yield function. It is shown graphically in fig. 6 (axisymmetric flow) for a range of values of f. Note that when f or $T_{\gamma\gamma}$ are zero, the yield function takes on a form of the von Mises yield function. This is quite reasonable, since the matrix material is a von Mises material.

When the conditions of eqns. 3.6 and minimization of $\dot{W}$ are not discarded, the approximate flow field becomes too complicated for analytical analysis (see ref. [17]). The integrals which define the components of $\underset{\sim}{\Sigma}$ can be carried out numerically, and the result is a class of yield functions which conform closely to the following analytic form:

$$\Phi = C_{eqv}\, T_{eqv}^2 + 2f \cosh\left(\frac{\sqrt{3}}{2} T_{\gamma\gamma}\right) - 1 - f^2 = 0 \tag{3.19}$$

C_{eqv} is an empirical function of f which varies with the direction of $\underset{\sim}{\dot{E}}$. (The subscript "eqv" indicates that it is a coefficient of T_{eqv}.) Its upper and lower limits are

$$C_{eqv} \cong (1 + 3f + 24f^6)^2 \text{ for } \dot{E}_{i3} = 0, \text{ plane strain,}$$

$$C_{eqv} = 1 \text{ for } \dot{E}_{11} = \dot{E}_{22}, \text{ axial symmetry.} \tag{3.20}$$

One possible contradiction which comes to mind is the case where plain strain and axial symmetry occur simultaneously, leading to two separate values of C_{eqv}. This can be resolved using the normal flow rule and eqn. 3.19:

$$\dot{E}_{33} = 0 \rightarrow T_{33} = \frac{1}{2} T_{\gamma\gamma},\ T_{11} = T_{22} \rightarrow T_{33} = T_{11}$$

$$\text{symmetry} \rightarrow T_{ij} = 0 \text{ for } i \neq j, \text{ cartesian coords.},\ T_{11} = T_{22} = T_{33} \rightarrow T_{eqv} = 0\ . \tag{3.21}$$

The coefficient of C_{eqv} in eqn. 3.19 is zero in this case, so C_{eqv} need not be well defined and there is no contradiction.

In fig. 5, eqn. 3.19 is compared to numerical solutions of eqns. 2.15 for plane strain. In fig. 6, the yield loci which result from application of eqn. 3.19 to three different types of $\dot{\underset{\sim}{E}}$ fields are shown. C_{eqv} for the intermediate curves ($\dot{E}_{33} = 1$, $\dot{E}' = 1$) was found by solving eqns. 2.15 for zero dilatation.

3b. Long Circular Cylindrical Voids - Plane Strain Flow with Rigid Section

The geometry considered here is the same as in section 3a. The flow field, however, has an important difference. For the case of plane strain ($\dot{E}_{33}=0$), part of the matrix remains rigid while the other part undergoes plastic flow to accommodate the macroscopic deformation. Also, the macroscopic boundary conditions now fall into the class of eqn. 2.2, rather than the simpler class of eqn. 3.1.

Plane strain deformation of a matrix containing cylindrical cavities has been studied via elastic-plastic finite elements [14,15] and (rigid-perfectly plastic) slip line theory [13], all of which support the idea of part of the matrix remaining rigid for some f and $\dot{\underset{\sim}{E}}$. The finite element solutions suggest that a radial plane might be a good approximation to the rigid-plastic boundary, and that the rigid region is symmetric around the principle axis along which there is the largest absolute strain rate.

In this section, primary consideration is given to the plane strain component of $\dot{\underset{\sim}{\varepsilon}}$. If desired, other components as derived in section 3a could be added on. A quarter section of the model is shown in fig. 7; wedges of rigid material are symmetric about the (2) axis. (This model can therefore be called the "wedge" model.) An approximate velocity field is constructed which allows for the rigid-plastic boundary, and is of the form of eqn. 2.19. ψ is the angle of the rigid-plastic boundary to the (2) axis, and takes on its optimum value (ψ_{opt}) when $\dot{W}$ is minimized for a given $\dot{\underset{\sim}{E}}$. (The minimization is carried out numerically.) Stresses are calculated via eqns. 2.21.

This formulation leads to some interesting numerical results, but does not lead to concise derived functional forms like eqns. 3.18 and 3.19. Because of this,

much detail of the type given in section 3a will not appear here. At the end of the section, an empirical functional form for the yield criterion will be presented which has some success in fitting the numerical data.

Consider the model in fig. 7. Boundary velocity is specified at $\alpha = 0$ and $\pi/2$, in terms of the boundary velocities V_1 and V_2. The general procedure is to find the microscopic velocity field in terms of V_1, V_2, and ψ, then to use eqn. 2.2 to obtain V_1 and V_2 for a given $\dot{\underset{\sim}{E}}$ and ψ. ψ is then varied to locate ψ_{opt}. As before, a yield locus results when $\underset{\sim}{\Sigma}$ is calculated (eqn. 2.21) for a range of $\dot{\underset{\sim}{E}}$.

The microscopic velocity field is constructed as follows: Start with general series solutions which obey the necessary symmetry conditions about the (1) axis ($\alpha=0$).

$$v_r = a_m r^m \cos(n_m \alpha) \quad , \quad v_\alpha = d_m r^m \sin(n_m \alpha) \qquad \text{sum over the } m \tag{3.22}$$

(m is both an index and an exponent.) Apply incompressibility, specialized to plane strain.

$$v_{r,r} + \frac{1}{r}(v_{\alpha,\alpha} + v_r) = 0 \rightarrow d_m = -(m+1)\frac{a_m}{n_m} \quad . \tag{3.23}$$

Equations 3.22 thus become

$$v_r = a_m r^m \cos(n_m \alpha), \; v_\alpha = -(m+1)\frac{a_m}{n_m} r^m \sin(n_m \alpha) \quad . \tag{3.24}$$

The rigid-plastic boundary requires that v_r and v_α be independent of r at $\alpha = \frac{\pi}{2} - \psi$. Terms with $m = 0$ obviously meet this condition. Because $\sin(x)$ and $\cos(x)$ are never both zero for the same value of x, meeting this condition for $m \neq 0$ requires that the coefficient of either $\sin(n_m\alpha)$ or $\cos(n_m\alpha)$ vanish for each value of m. This is fulfilled nontrivially for $a_m \neq 0$ only when $m = -1$. Equations 3.24 thus become

$$v_r = a_o \cos(n_o\alpha) + a_{-1} r^{-1} \cos(n_{-1}\alpha)\ ,\ n_{-1} = \frac{1}{\left[1-\frac{2\psi}{\pi}\right]},\ v_\alpha = -\frac{a_o}{n_o}\sin(n_o\alpha) \quad (3.25)$$

The next step is to determine n_o, a_o, and a_{-1} in terms of V_1 and V_2. The process is simplified by the following changes of variable:

$$V_1^N = V_1 b^{-1}\ ,\ V_2^N = V_2 b^{-1},\ A_o = \frac{a_o}{V_2^N b}\ ,\ A_{-1} = \frac{a_{-1}}{V_1^N b^2}\ . \quad (3.26)$$

The boundary conditions then give, using eqns. 3.25

$$\text{at}\begin{bmatrix} r=b, \\ \alpha=0 \end{bmatrix} v_r = V_1^N b \rightarrow V_1^N = A_o V_2^N + A_{-1} V_1^N \quad (a)$$

$$\text{at}\begin{bmatrix} r=b, \\ \alpha=\frac{\pi}{2}-\psi \end{bmatrix} v_r = V_2^N b \cos(\psi) \rightarrow \cos(\psi) = A_o \cos\left[n_o\left(\frac{\pi}{2}-\psi\right)\right] \quad (b) \quad (3.27)$$

$$v_\alpha = V_2^N b \sin(\psi) \rightarrow \sin(\psi) = \frac{-A_o}{n_o}\sin\left[n_o\left(\frac{\pi}{2}-\psi\right)\right] \quad (c)$$

For a given ψ, eqns. 3.27 b and c can be solved numerically for n_o and A_o. Note that A_o is a function of ψ only, and not of V_1^N and V_2^N. A_{-1} is, from eqn. 3.27a, expressible in terms of A_o, V_1^N, and V_2^N.

Using λ as defined in eqn. 3.10d, $\underset{\sim}{v}$ can now be written as

$$v_r = b[A_o V_2^N \cos(n_o\alpha) + A_{-1} V_1^N \lambda^{-1/2} \cos(n_{-1}\alpha)]\ ,\quad v_\alpha = -b\frac{A_o}{n_o} V_2^N \sin(n_o\alpha). \quad (3.28)$$

For a given ψ, v_r and v_α are linear functions of V_1^N and V_2^N. Noting that the rigid section has the velocity field

$$v_r = V_2^N \sin(\alpha),\quad v_\alpha = V_2^N \cos(\alpha)\ , \quad (3.29)$$

a linear homogeneous relationship between $\underset{\sim}{V}^N$ and $\dot{\underset{\sim}{E}}$ (for constant ψ) can be obtained via eqn. 2.2. (The surface integral in eqn. 2.2 is, of course, taken over both the rigid and the plastic sections.) $\underset{\sim}{V}^N$, $\underset{\sim}{v}$, $\dot{\underset{\sim}{\varepsilon}}$, and thus $\dot{W}$ are derivable from $\dot{\underset{\sim}{E}}$ for a given ψ. A numerical procedure then locates $\dot{W}_{min}$ and ψ_{opt}.

It is assumed that the yield function for this type of flow field takes a general form similar to that in the previous section:

$$\Phi = T_{eqv}^2 + \mathcal{F}(f, T_{\gamma\gamma}) = 0 \ , \tag{3.30}$$

where $\mathcal{F}$ is some function. Therefore, for plane strain deformation,

$$T'_{33} = 0 \rightarrow T_{eqv} = |T_{22} - T_{11}| \tag{3.31}$$

so yield loci for plane strain can be calculated without computing the T_{i3} .

These yield loci are shown in figs. 8. In comparing these curves with those obtained for fully plastic flow, it is immediately apparent that the wedge model gives a more negative slope in the lower range of $T_{\gamma\gamma}$. By the normal flow rule, the wedge model thus predicts more dilatation in this range. Considering that the effect of a rigid wedge would be to inhibit contraction in the (1) direction (see fig. 7), this is reasonable. The wedge yield loci have the desirable property of convexity to the origin (see section 2).

Given the same matrix material and void geometry and the same boundary value problem, each type of yield function will give a different solution. The correct choice is the solution which gives the best upper bound (the lowest dissipation). This choice should also reflect which tvpe of microscopic velocity field more closely resembles the actual field. Its point in stress space (on the "correct" yield function) will lie closer to the origin than the competing solution. Because the curves in fig. 8b intersect, a preferred yield locus over all stress space would consist of segments of the wedge and fully plastic yield functions.

The flow direction predicted (via normality) by the actual yield locus should obey the following symmetry conditions. For zero biaxial stress ($T_{\gamma\gamma}=0$), there should be no dilatation ($\dot{E}_{\gamma\gamma}=0$) , and for an axisymmetric stress state, the flow should also be axisymmetric. (In plane strain, the latter corresponds to

$T_{eqv} = 0$. See eqn. 3.21.) These two conditions on the yield loci are satisfied by the fully plastic model, but not by the inherently asymmetric wedge model. Therefore, if the approximate fully plastic yield function dominates (is closer to the origin) at $T_{\gamma\gamma} = 0$ and at $T_{eqv} = 0$, the models gain credibility.

This is indeed the case over the entire range of f when the yield locus which resulted from the refined fully plastic flow field (eqn. 3.19) is used, but is not the case for the unrefined yield locus (eqn. 3.18). The importance of a refinement procedure is thus underscored. Note that the wedge flow field was also refined by varying the angle of the rigid-plastic boundary.

As noted previously, no functional form for the yield locus emerges from calculations using the wedge flow field. However, some success has been achieved in fitting the following empirical form to the data:

$$\Phi = 0 = T_{eqv}^2 - [B_o + B_1 T_{GH} + B_2 T_{GH}^2] \quad , \quad T_{GH} \equiv \frac{1}{2} T_{\gamma\gamma} \tag{3.32}$$

The coefficients B_o, B_1, and B_2 are constant for a given f. They were determined by fitting eqn. 3.32 to three numerical data points, spaced as evenly as possible over the computed yield locus. See figure 9a.

For values of f between those for which numerical data is available, approximate yield curves can be obtained by interpolation of the B_i over f. Figure 9b shows the computed values of B_o, B_1, and B_2 as functions of f, with solid lines showing the linear interpolation.

In a paper by Nagpal, McClintock, Berg, and Subhuti [13], plane strain slip line solutions for bands of evenly spaced cylindrical cavities (long axis in the plane strain direction) are developed. The cross sections of the cavities considered included slits at various angles, and circular holes. The bands have

zero extension in the transverse direction, a result of a fracture criterion being investigated there. For their cylindrical cavities with circular cross sections, an analogy can be made to the cylindrical cavity models developed here. The slip line solutions are done for various ratios of shear traction to normal traction (on the band), so with a bit of manipulation, the results generated here can be compared directly with theirs. The counterclockwise rotation from principle axes to axes in which $\dot{E}_{11} = 0$ is given by

$$\tan^2(\theta) = -\frac{\dot{E}_{11}}{\dot{E}_{22}} \quad . \tag{3.33}$$

Then, where the superscript * denotes quantities in coordinates reached by that rotation, and subscripts "n" and "s" denote "normal" and "shear",

$$\Sigma_n = \Sigma^*_{22} = \sin^2(\theta)\Sigma_{11} + \cos^2(\theta)\Sigma_{22}$$

$$\Sigma_s = \Sigma^*_{21} = \sin(\theta)\cos(\theta)(\Sigma_{11}-\Sigma_{22}) \tag{3.34}$$

Any comparison of results require an interpretation of the geometric parameters in ref. [13] in terms of void volume fraction f. Their parameters are P, the void radius, and L, half the intervoid spacing. Extending their one dimensional void array into a two dimensional square array, and considering the two most likely band directions (horizontal and diagonal directions in the square array), one can say that

$$\frac{\pi P^2}{4L^2} \leq f \leq \frac{\pi P^2}{2L^2}, \quad f \approx \frac{3}{8}\pi\left(\frac{P}{L}\right)^2 \quad . \tag{3.35}$$

The intermediate value is used in the comparisons.

There are three types of data sets in fig. 10. The points connected by solid lines and denoted by values of P/L are from the slip line model. The dashed lines and the unconnected points represent fully plastic and wedge yield

functions respectively, transformed via eqns. 3.34. Note that

$$\frac{P}{L} = 0.123, \quad \frac{3}{8}\pi\left(\frac{P}{L}\right)^2 = 0.0178$$

$$\text{" } \quad 0.208 \quad \text{" } \quad 0.051 \simeq 0.05 \tag{3.36}$$

$$\text{" } \quad 0.50 \quad \text{" } \quad 0.294 \simeq 0.30$$

As can be seen from fig. 10, the wedge yield locus is a much better match than the fully plastic yield locus to the results of the slip line model, particularly in slope. (Note that the interpretation of f in terms of P/L is rather arbitrary, and could be changed considerably.) The slope is the most important factor, because the direction of $\dot{\underset{\sim}{E}}$ is determined via normality. For this reason, the similarity in slope of the slip line and wedge yield loci is particularly satisfying, and helps to justify the development of the wedge model.

4a. Spherical Voids, Fully Plastic Flow

This void geometry, shown in fig. 3., is meant to represent a limit of void shape different from the long circular cylinder. Voids of spheroidal shape can result from decohesion or breakage of similarly shaped second phases during deformation [1-6]. Nucleation without second phases has also been seen to occur at grain boundary misfits due to straining [18]. Sintered compacts of metal powder can be specially prepared so that they contain approximately equiaxed voids [19,20]. Voids can also be present by accident, through faulty processing.

Many parts of this analysis are similar to parts of section 3a. The spherical geometry is simpler to work with than the cylindrical geometry because there are no preferred axes. A refinement procedure analogous to that carried out for the cylinder was carried out for the sphere; in contrast, little change in the calculated yield loci resulted. For this reason, a refinement procedure will not be discussed here.

Because there are no preferred directions, the approximate microscopic velocity field will be broken up into two parts (as in ref. [9]); shape change at constant volume ($\underset{\sim}{v}^s$), and volume change at constant shape ($\underset{\sim}{v}^v$). The total field is then

$$\underset{\sim}{v} = \underset{\sim}{v}^s + \underset{\sim}{v}^v \tag{4.1}$$

The $\dot{\underset{\sim}{\varepsilon}}$ field calculated from $\underset{\sim}{v}$ must, as before, be incompressible, and $\underset{\sim}{v}$ must meet external boundary conditions put in terms of the $\dot{E}_{ij}$.

$$v_i\Big|_S = \dot{E}_{ij}x_j\Big|_S \text{ (cartesian words.)} \tag{4.2}$$

This is the same type of boundary condition used for the fully plastic cylindrical model. It can be met by a simple incompressible flow field which relates $\underset{\sim}{v}^s$ to $\dot{\underset{\sim}{E}}'$ (the deviatoric part of $\dot{\underset{\sim}{E}}$) and $\underset{\sim}{v}^v$ to $\dot{E}_{kk}$:

$$v_i^s = \dot{E}'_{ij}x_j \rightarrow \dot{\varepsilon}^s_{ij} = \dot{E}'_{ij} \quad , \quad v_r^v = \frac{\dot{E}_{kk}}{3}\frac{b^3}{r^2} \quad , \quad v_\theta^v = v_\phi^v = 0$$
$$\rightarrow \dot{\varepsilon}^v_{rr} = -\frac{2}{3}\left(\frac{b}{r}\right)^3 \dot{E}_{kk} = -2\dot{\varepsilon}^v_{\theta\theta} = -2\dot{\varepsilon}^v_{\phi\phi} \quad , \quad \dot{\varepsilon}^v_{r\theta} = \dot{\varepsilon}^v_{r\phi} = \dot{\varepsilon}^v_{\theta\phi} = 0 \quad . \tag{4.3}$$

Adding the two components of $\dot{\underset{\sim}{\varepsilon}}$ gives

$$\dot{\underset{\sim}{\varepsilon}} = \dot{\underset{\sim}{\varepsilon}}^s + \dot{\underset{\sim}{\varepsilon}}^v \quad , \quad \dot{\varepsilon}_{ij} = \dot{E}'_{ij} + \frac{1}{3}\dot{E}_{kk}h_{ij} \quad . \tag{4.4}$$

In spherical coordinates,

$$h_{rr} = -2\left(\frac{b}{r}\right)^3 = -2h_{\theta\theta} = -2h_{\phi\phi} \quad , \quad h_{ij}\Big|_{i\neq j} = 0 \quad , \tag{4.5}$$

and in cartesian coordinates,

$$h_{ij} = (\delta_{ij} - 3n_in_j)\left(\frac{b}{r}\right)^3 \quad , \quad r^2 = x_1^2 + x_2^2 + x_3^2 \quad ,$$
$$n_i = \frac{x_i}{r} = \text{cartesian components of unit normal to sphere of radius } r \quad . \tag{4.6}$$

Carrying out eqn. 2.15 for this simple $\dot{\underset{\sim}{\varepsilon}}$ field, and separating into deviatoric and hydrostatic components gives

$$\Sigma'_{ij} = \frac{1}{V}\int_V s_{ij}(\dot{\underset{\sim}{\varepsilon}})dV \quad , \quad \Sigma_{nn} = \frac{1}{V}\int_V s_{k\ell}(\dot{\underset{\sim}{\varepsilon}})h_{k\ell}dV \quad . \tag{4.7}$$

Using $s_{nn} = 0$ and eqn. 4.5, one can write

$$\Sigma_{nn} = \frac{1}{V}\int_V \frac{3}{2}s_{rr}(\dot{\underset{\sim}{\varepsilon}})h_{rr}dV \quad . \tag{4.7}$$

Equations 4.7 can be solved approximately in a manner very similar to that used for the fully plastic cylindrical model. As before, σ_o is presumed constant with respect to geometry.

The calculations are done in detail in ref. [17], and were originally suggested in ref. [22]. Some of the intermediate expressions which are similar to those in the cylindrical example are

$$\dot{\varepsilon}_{ij}\dot{\varepsilon}_{ij} = \dot{E}'_{ij}\dot{E}'_{ij} - 2\dot{E}_{nn}\dot{E}'_{rr}\left(\frac{b}{r}\right)^3 + \frac{2}{3}\dot{E}^2_{nn}\left(\frac{b}{r}\right)^6 , \quad \lambda = \left(\frac{r}{b}\right)^3 , \quad x = \lambda^{-1}$$

$$dV = r^2\sin(\phi)d\phi d\theta dr \equiv r^2 d\Omega dr , \quad \frac{1}{V}\int_V dV = \frac{1}{4\pi}\int_\Omega \int_f^1 d\lambda d\Omega \qquad (4.8)$$

$$\mu = \dot{E}'_{rr}\left(\frac{2}{3}\dot{E}'_{k\ell}\dot{E}'_{k\ell}\right)^{-\frac{1}{2}} , \quad \int_\Omega \mu d\Omega = 0 \ . \ \Omega \text{ is a solid angle.}$$

As before, the integrands are expanded into polynomials in μ ; the multiple integrals can then be carried out approximately. Equations similar to 3.18 and 3.19 are the result. To first order in μ , the yield function for the spherical geometry and this simple flow field is

$$\Phi = T^2_{eqv} + 2f\cosh\left(\frac{1}{2}T_{nn}\right) - 1 - f^2 = 0 \qquad (4.9)$$

This yield function is shown in fig. 11, along with a solution to second order in μ and some data points resulting from numerical solution of the stress integrals. It can be seen that the first order solution is very close to the second order solution. Unlike the case of the cylinder, this yield function appears rather insensitive to the direction of $\dot{\underset{\sim}{E}}$. Given the geometric isotropy of the model, this is not unexpected.

4b. Spherical Voids - Flow with Rigid Section

The model used here is a spherical analog of the model used in section 3b, and is limited to axisymmetric deformation. The rigid sections are idealized as truncated circular cones capped with spherical sections, whose axes coincide with the tensile axis. ψ is the angle between the tensile axis and the cone wall, and is used to optimize the flow field via minimization of $\dot{W}$. See fig. 4.

The form of the calculations for this model is very similar to that in section 3a, as are the solutions. Again, the calculations do not lead to a derived functional form, but there is some success in fitting the numerical results to an equation similar in form to eqn. 3.32.

In the model, the (3) axis is the tensile direction, and the (1) and (2) axes are the transverse directions which are equivalent due to symmetry. Figure 7 can therefore be used to illustrate important quantities, once the index "3" replaces the index "2".

Because the similarities are so great, the reader should refer to section 3b (or ref. [17]) for details of the calculation. Some differences with the cylindrical model should, however, be noted. These include the incompressibility equation for the spherical geometry (with axial symmetry):

$$r v_{r,r} + [2v_r - v_\alpha \tan(\alpha) + v_{\alpha,\alpha}] = 0 \quad . \tag{4.10}$$

When eqns. 3.22 are inserted, the terms $\sin(n_m \alpha) \tan(\alpha)$ appear. Nontrivial equations result only for special values of n_m; where trigonometric identities such as

$$\sin(2\alpha) \tan(\alpha) = 1 - \cos(2\alpha) \ , \quad \sin(4\alpha) \tan(\alpha) = -1 + 2\cos(2\alpha) - \cos(4\alpha) \tag{4.11}$$

apply. (In the calculations, n_m is taken no larger than 4.) Because of this, $\underset{\sim}{y}$ takes on a slightly different form than in the cylindrical case.

As before, the $\underset{\sim}{T}$ field is calculated via eqn. 2.21. The yield function is assumed to have the form

$$\phi = T_{eqv}^2 + \mathcal{F}(f, T_H) = 0 \quad , \tag{4.12}$$

where, due to axial symmetry,

$$T_{eqv} = |T_{33} - T_{11}| \quad , \quad T_H \equiv \frac{1}{3} T_{kk} = \frac{1}{3} (2T_{11} + T_{33}) \tag{4.13}$$

Values of T_{eqv} vs. T_H for several values of f are shown in fig. 12, and compared with yield functions derived from fully plastic flow fields. It should be noted that the symmetry arguments cited in section 3b do not apply in the spherical case. It is therefore not expected that the fully plastic yield function will dominate at $T_H = 0$ for all values of f. (It does dominate, however, for very small values of f; this is to be expected.) Also note that the yield loci which result from the "rigid cone" model are convex.

The yield loci derived from the rigid cone model can also be fit to eqn. 3.32. Calculated values of B_o, B_1, and B_2 are shown in fig. 13.

Summary

A method has been developed for calculating approximate yield loci via an upper bound approach for porous ductile materials. This method was applied to material models with simplified matrix and void geometries, and with two different types of matrix flow field approximations. The results were two different types of upper bound yield functions. Comparison with somewhat similar work by other authors was encouraging.

The approximate yield functions developed here show the important property of plastic dilatation; a property not evident in ordinary incompressible plasticity formulations. Because the dilatancy increases with the hydrostatic component of stress, the yield functions (and flow rules) developed here could lead to better understanding of plastic behavior in regions of high hydrostatic stress (e.g., necks in sheets and bars, and near the tips of cracks and notches).

As examined here, plastic dilatation requires that some porosity be present. When this is not initially the case, porosity can sometimes be nucleated during straining at second phases in a ductile matrix or at grain boundary misfits. Nucleation at second phases is examined in ref. [17], and will be discussed in the next paper of this series.

Acknowledgment

The author gratefully acknowledges the financial support of the Energy Research and Development Agency under contract AT(11-1)-3084, and the initial support of a National Science Foundation Traineeship during the course of the work leading to this paper.

This work is based on the first part of the author's Ph.D. thesis (1975, Brown University). The contribution of the thesis advisor, Professor J. R. Rice, is also gratefully acknowledged.

The author also gratefully acknowledges Leone Cargill and Diane Minter in the preparation of the manuscript.

References

[1] Gurland, J., and Plateau, J. 1963 "The Mechanism of Ductile Rupture of Metals Containing Inclusions" Transactions of the A.S.M. 56, pp. 443-454.

[2] Beachem, C. D. 1963 "An Electron Fractographic Study of the Influence of Plastic Strain Conditions Upon Ductile Rupture Processes in Metals" Transactions of the A.S.M. 56, pp. 318-326.

[3] Bluhm, J. I., and Morrissey, R. J. 1965 "Fracture in a Tensile Specimen" in International Conference on Fracture, Sendai, Japan.

[4] Darlington, H. 1971 "Ductile Fracture Under Axisymmetric Stresses in Electrolytic Iron and Spheroidized Low-Carbon Steel" Ph.D. thesis, Dept. of Metallurgy and Materials Science, Lehigh University, Bethlehem, Pa.

[5] Liu, C. T., and Gurland, J. 1968 "The Fracture Behavior of Spheroidized Carbon Steels" Transactions of the A.S.M. 61, pp. 156-167.

[6] Low, J. R., et al 1972 "Investigation of the Plastic Fracture of Aluminum Alloys, High Strength Steels" NASA Technical Reports nos. 2,3,4 NGR 39-087-003, Carnegie-Mellon University.

[7] Hill, R. 1950 The Mathematical Theory of Plasticity, The University Press, Oxford.

[8] McClintock, F. A. 1968 "A Criterion for Ductile Fracture by the Growth of Holes" Journal of Applied Mechanics 35, pp. 363-371.

[9] Rice, J. R., and Tracey, D. M. 1969 "On the Ductile Enlargement of Voids in Triaxial Stress Fields" J. Mech. Phys. Solids 17, pp. 201-217.

[10] Kahlow, K. J., and Avitzur, B. 1969 "Void Behavior as Influenced by Deformation and Pressure" report to the American Iron and Steel Institute. Lehigh University.

[11] Bishop, J. F. W., and Hill, R. 1951 "A Theory of the Plastic Distortion of a Polycrystalline Aggregate Under Combined Stresses", Phil. Mag. 42, pp. 414-427.

[12] Berg, C. A. 1969 "Plastic Dilation and Void Interaction" in the Proceedings of the Batelle Memorial Institute Symposium on Inelastic Processes in Solids, pp. 171-209.

[13] Nagpal, V., McClintock, F. A., Berg, C. A., and Subudhi, M. 1972 "Traction-Displacement Boundary Conditions for Plastic Fracture by Hole Growth" in the Intl. Symposium on Foundations of Plasticity, vol. 1 (A. Sawczuk, ed.) pp. 365-385.

[14] Needleman, A. 1972 "Void Growth in an Elastic Plastic Medium" Journal of Applied Mechanics 39, pp. 964-970.

[15] Haward, R. N., and Owen, D. R. J. 1973 "The Yielding of a Two Dimensional Void Assembly in an Organic Glass" Journal of Materials Science 8, pp. 1136-1144.

[16] Timoshenko, S. P., and Goodier, J. N. 1934, 1951 Theory of Elasticity, p. 78.

[17] Gurson, A. L. 1975 "Plastic Flow and Fracture Behavior of Ductile Materials Incorporating Void Nucleation, Growth, and Interaction" Ph.D. thesis, Division of Engineering, Brown University, Providence Rhode Island.

[18] Bauer, R. W., and Wilsdorf, H. G. F. 1973 "Void Initiation in Ductile Fracture" Scripta Metallurgica 7, pp. 1213-1220.

[19] Edelson, B. I., and Baldwin, W. M. 1962 "The Effect of Second Phases on the Mechanical Properties of Alloys" Transactions of the A.S.M.55, pp. 230-250.

[20] Rostoker, W. and Liu, S. Y. K. 1970 "The Influence of Porosity on the Ductility of Sintered Brass" Journal of Materials J.M.L.S.A. 5, pp. 605-617.

[21] C.R.C. Standard Math Tables The Chemical Rubber Co., Cleveland, Ohio.

[22] Rice, J. R., 1972 private communication.

Appendix - The Normal Flow Rule and Convexity

The normal flow rule arises from the definition of $\underset{\sim}{\Sigma}$ (eqn. 2.15) and the fact that the dissipation $\dot{W}$ is homogeneous of degree one in $\dot{\underset{\sim}{E}}$ (eqn. 2.14). These lead to

$$\delta\Sigma_{ij}\dot{E}_{ij} = 0 \tag{A.1}$$

for $\delta\underset{\sim}{\Sigma}$ emanating from $\underset{\sim}{\Sigma}$ on the yield surface, and directed along the yield surface. This means that the components of $\dot{\underset{\sim}{E}}$ are proportional to the components of the normal to the yield surface in stress space, i.e.,

$$\dot{E}_{ij} = \Lambda \frac{\partial \Phi}{\partial \Sigma_{ij}} \quad . \tag{A.2}$$

Λ is a macroscopic scalar, determined either by boundary conditions in $\dot{\underset{\sim}{E}}$, or $d\underset{\sim}{\Sigma}$ and the hardening behavior of the aggregate. See fig. 14a.

Convexity as well as normality can be proven when a maximum plastic work principle (eqns. 2.8, 2.17 and 2.18) exists. The proof is illustrated in fig. 14b, where a concavity in the yield surface is shown to violate the principle.

Now; consider the yield functions shown in figs. 5,6,8,9,11, and 12, where the axes are functions of stress other than the tensor components. The questions to be discussed below are when and how the principles of convexity and normality apply to yield functions expressed in terms of those functions of stress.

In the general case, the answer lies in the proofs of convexity and normality in chapter 2. They will work for any strain rate measure in which $\dot{W}$ is homogeneous of degree one, when the stress measures are work conjugates to those strain rate measures. Acceptible stress and strain rate measures can be found by manipulating the expression for $\dot{W}$. For example:

$$\dot{W} = \Sigma_{ij}\dot{E}_{ij} = (\Sigma'_{ij} + \frac{1}{3}\Sigma_{kk}\delta_{ij})(\dot{E}'_{ij} + \frac{1}{3}\dot{E}_{nn}\delta_{ij}) = \Sigma'_{ij}\dot{E}'_{ij} + \frac{1}{3}\Sigma_{kk}\dot{E}_{nn} \qquad (A.3)$$

For the special case of axially symmetric distributions of the principle values of $\underset{\sim}{\Sigma}$ and $\underset{\sim}{\dot{E}}$, this becomes

$$\dot{W} = \Sigma_{eqv}\dot{E}_{eqv} + \frac{1}{3}\Sigma_{kk}\dot{E}_{nn}, \text{ where } \dot{E}_{eqv} = (\frac{2}{3}\dot{E}'_{ij}\dot{E}_{ij})^{1/2}. \qquad (A.4)$$

The normal flow rule then gives

$$\dot{E}_{eqv} = \Lambda \frac{\partial \bar{\Phi}}{\partial \Sigma_{eqv}} \quad , \quad \dot{E}_{nn} = \Lambda \frac{\partial \bar{\Phi}}{\partial(\frac{1}{3}\Sigma_{kk})} \quad . \qquad (A.5)$$

The flow rule is also valid in terms of $\underset{\sim}{T}$, with the factor σ_o taken account of in Λ:

$$\dot{E}_{eqv} = \Lambda \frac{\partial \bar{\Phi}}{\partial T_{eqv}} \text{, etc.} \qquad (A.6)$$

Referring to figs. 11 and 12, the ratios of the strain rate measures is equal to the slope of the normal to the yield function:

$$\frac{\dot{E}_{eqv}}{\dot{E}_{nn}} = \left.\frac{dT_{eqv}}{dT_H}\right|_{\substack{\text{normal to} \\ \bar{\Phi}=0}} \quad , \quad T_H \equiv \frac{1}{3}T_{kk} \qquad (A.7)$$

A very simple interpretation of normality thus results for the spherical void model when $\underset{\sim}{\Sigma}$ and $\underset{\sim}{\dot{E}}$ are axisymmetric.

Suppose that the yield function is constrained to be a function of the first two stress invariants, as in eqns. 3.18, 3.19, and 3.32 (the approximate yield function for the spherical model):

$$\bar{\Phi} = \bar{\Phi}(T_{eqv}, T_{kk}, f) = 0 \quad . \qquad (A.8)$$

Applying the normal flow rule then gives

$$\dot{E}_{ij} = \Lambda \left(\frac{\partial \bar{\Phi}}{\partial T_{eqv}} \frac{3}{2} \frac{T'_{ij}}{T_{eqv}} + \frac{\partial \bar{\Phi}}{\partial T_{kk}} \delta_{ij} \right)$$

$$\rightarrow \dot{E}_{eqv} = \Lambda \frac{\partial \bar{\Phi}}{\partial T_{eqv}} \quad , \quad \dot{E}_{nn} = \Lambda \frac{\partial \Phi}{\partial T_H} \quad . \tag{A.9}$$

The simple interpretation is thus invariant to $\dot{\underset{\sim}{E}}$ when eqn. A.8 is true.

The approximate yield functions derived for the cylindrical model are expressed in terms of T_{eqv} and $T_{\gamma\gamma}$; $T_{\gamma\gamma}$ is used in place of T_{kk} because it is a more logical choice as the driving force for dilation in the cylindrical geometry. Equation A.3 can apply in this situation when the stress is constrained such that $T_{\gamma\gamma}$ is expressible in terms of T_{kk}, such as for plane stress $(T_{i3} = 0,\ i = 1, 3)$. When the yield function takes the form

$$\bar{\Phi} = \bar{\Phi}(T_{eqv}, T_{\gamma\gamma}, f) = 0 \quad , \tag{A.10}$$

plane strain is also in this category because by normality ,

$$\dot{E}_{33} = 0 \rightarrow T'_{33} = 0 \rightarrow T_{33} = \frac{1}{2} T_{\gamma\gamma}, \; T_{kk} = \frac{3}{2} T_{\gamma\gamma} \quad . \tag{A.11}$$

Equation A.3 can then be written as follows, when $T_{22} > T_{11}$ and $\dot{E}_{22} > \dot{E}_{11}$

$$\dot{W} = \sigma_o \left[T_{eqv} (\dot{E}_{22} - \dot{E}_{11}) + \frac{1}{2} T_{\gamma\gamma} \dot{E}_{\gamma\gamma} \right]$$

$$\text{where } (\dot{E}_{22} - \dot{E}_{11}) = \left[E^2_{eqv} - \frac{1}{9} \dot{E}_{\gamma\gamma} \right]^{1/2} \tag{A.12}$$

$$\text{so, } \left[E^2_{eqv} - \frac{1}{9} E^2_{\gamma\gamma} \right]^{1/2} = \Lambda \frac{\partial \bar{\Phi}}{\partial T_{eqv}} \qquad E_{\gamma\gamma} = \Lambda \frac{\partial \bar{\Phi}}{\partial (\frac{1}{2} T_{\gamma\gamma})} \quad .$$

These results can also be obtained from eqn. A.10 using the normal flow rule (as in eqns. A.8 and A.9), provided that it is recognized that

$$\frac{\partial T_{\gamma\gamma}}{\partial T_{33}} = 0 \qquad \text{(A.13)}$$

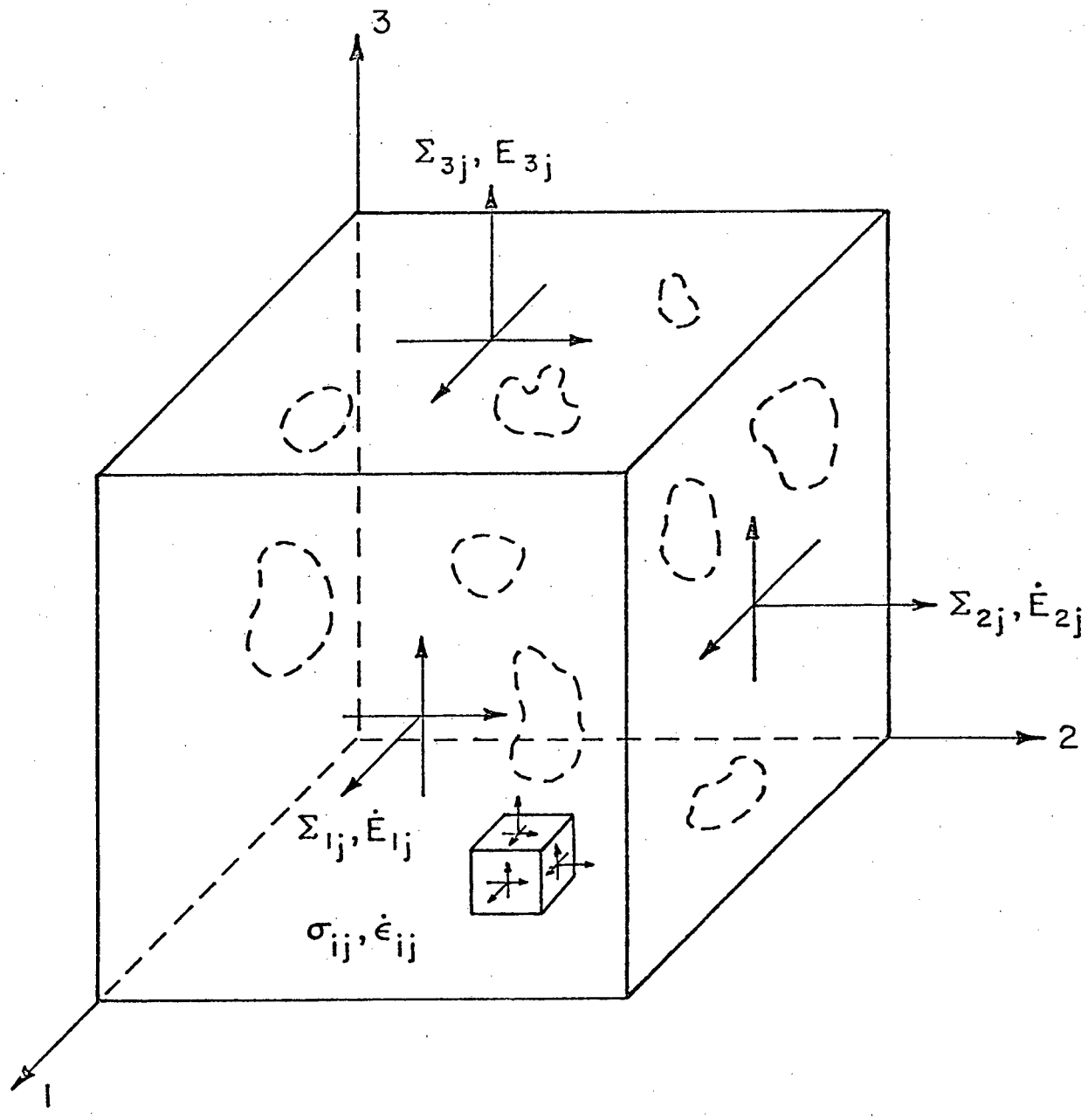

VOID-MATRIX AGGREGATE
RANDOM VOID SHAPES AND ORIENTATIONS
MACROSCOPIC AND MICROSCOPIC TENSOR QUANTITIES

FIGURE 1

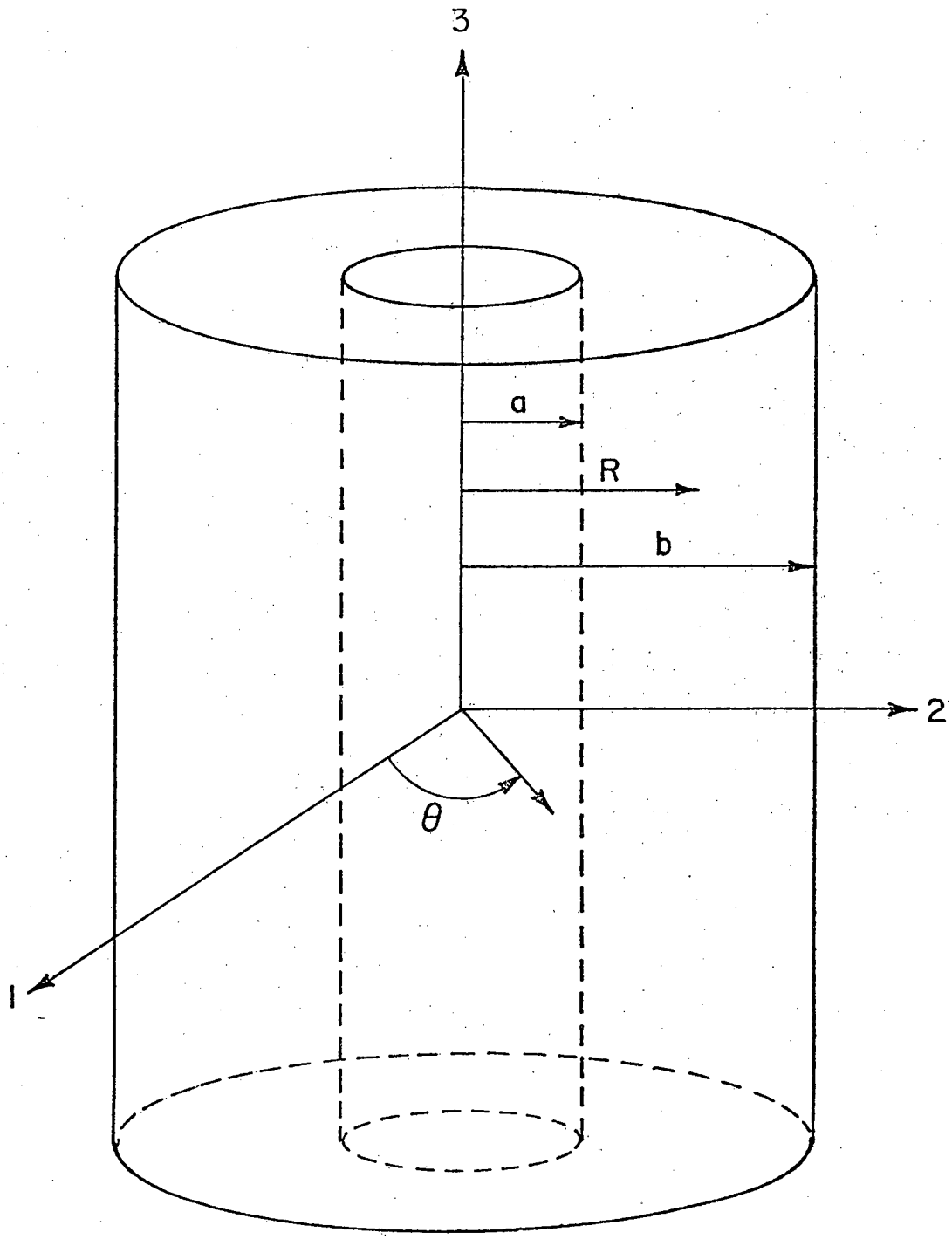

LONG CIRCULAR CYLINDRICAL VOID IN A MATRIX OF RIGID-PERFECTLY PLASTIC VON MISES MATERIAL

FIGURE 2

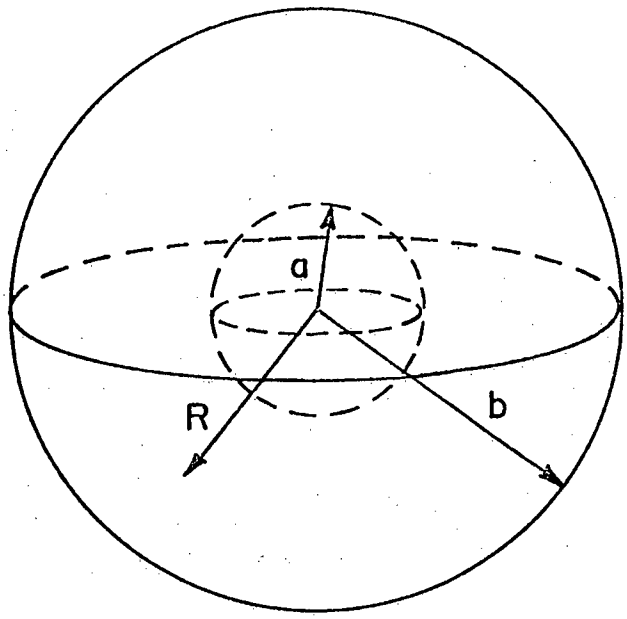

SPHERICAL MODEL

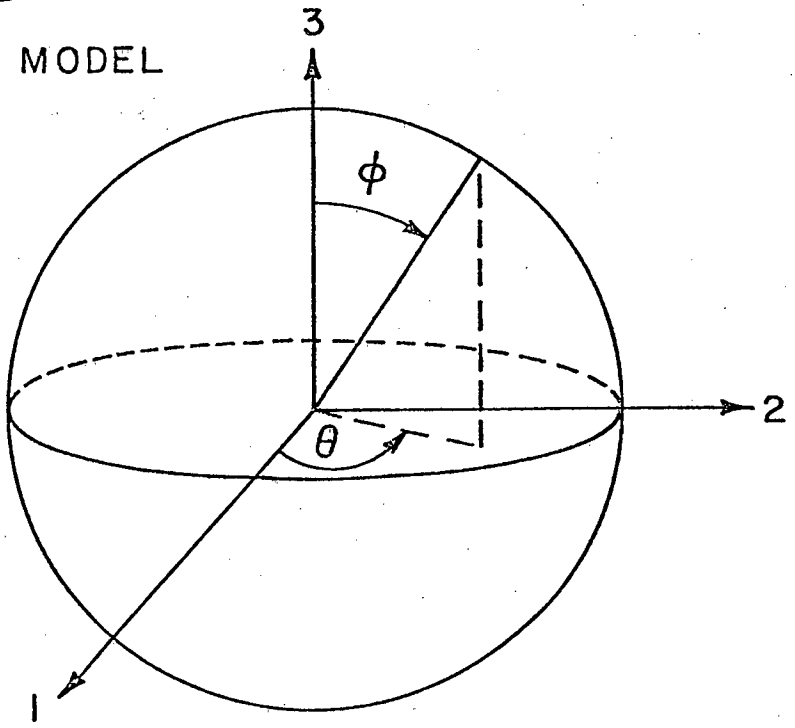

UNIT SPHERE
PRINCIPAL AXIS SYSTEM

FIGURE 3

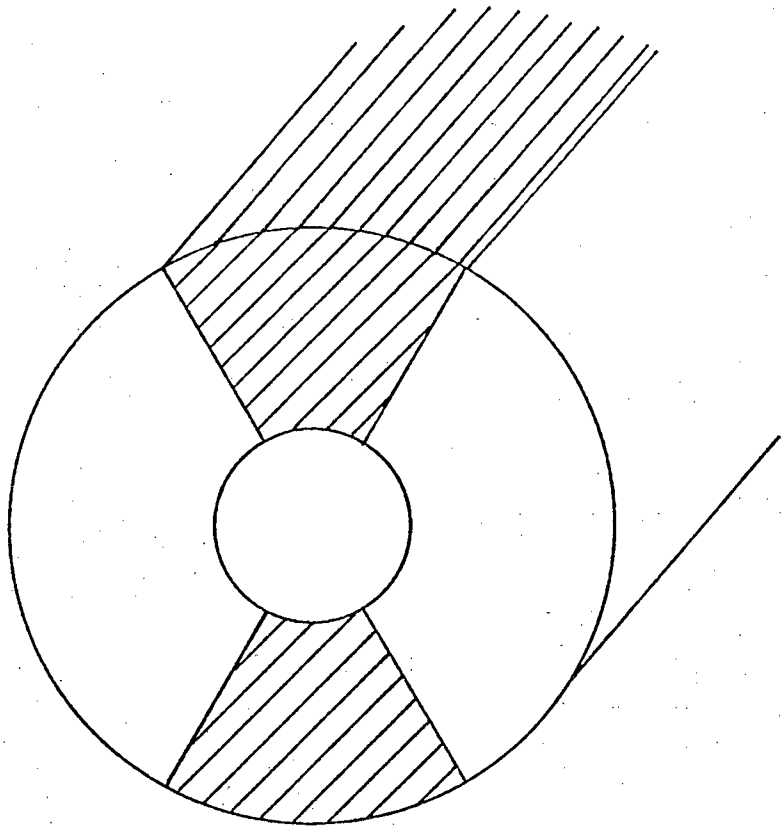

CYLINDRICAL MODEL
RIGID WEDGE
PLANE STRAIN

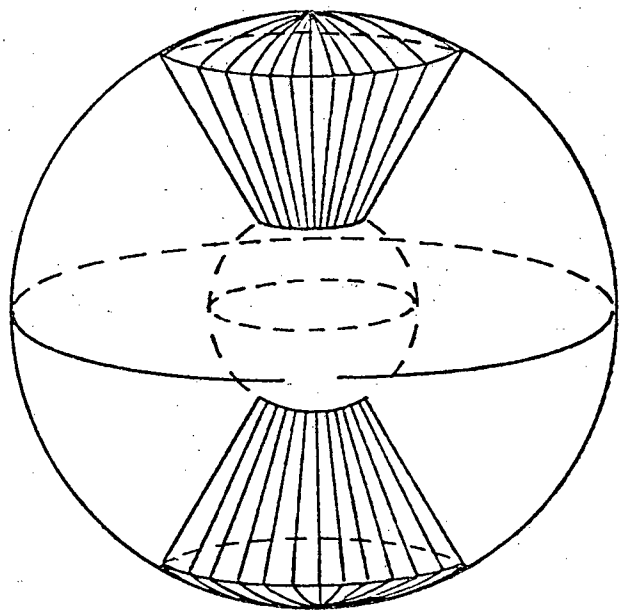

SPHERICAL MODEL
RIGID CONE
AXISYMMETRIC FLOW

FIGURE 4

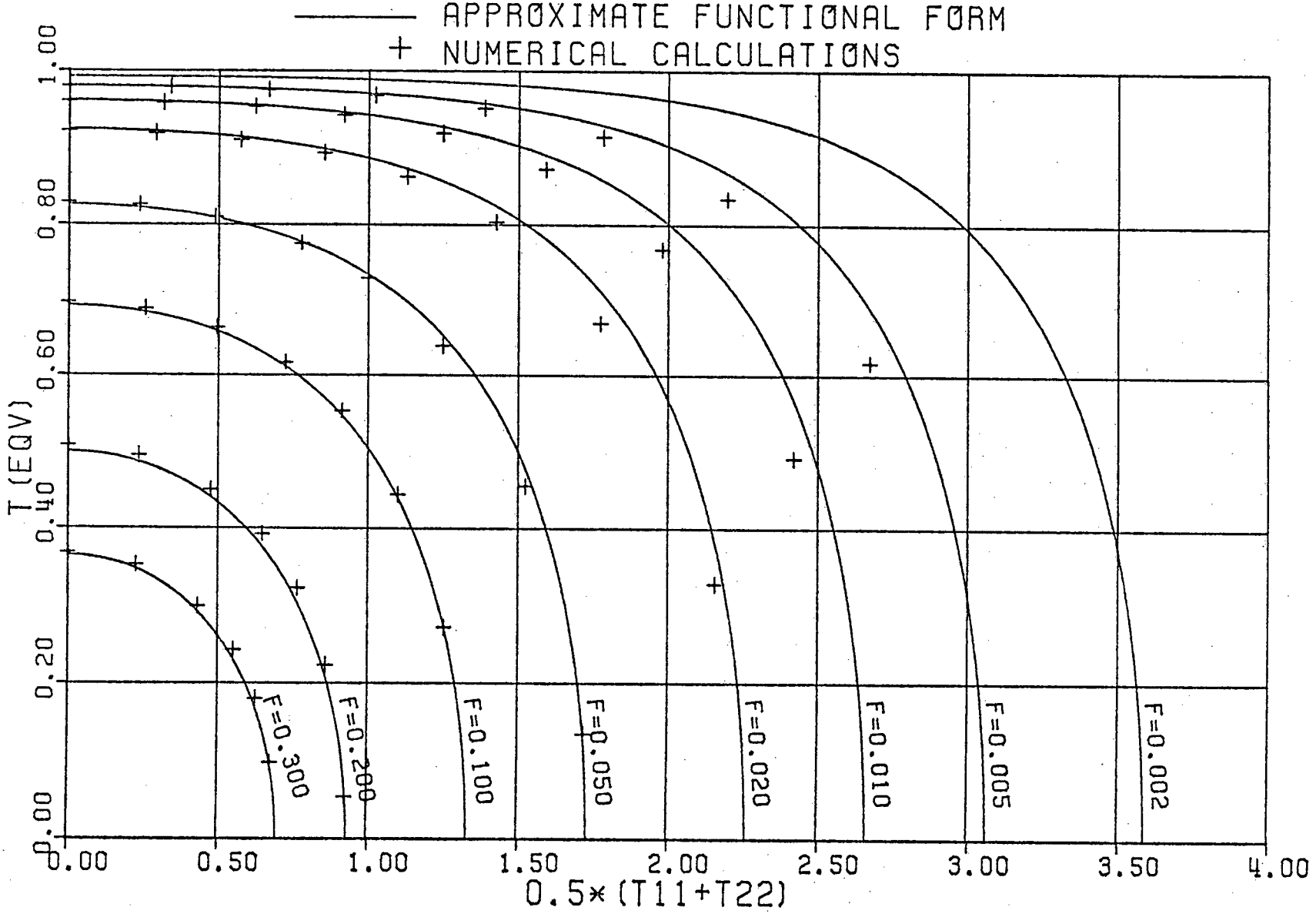
CYLINDRICAL VØIDS, FULLY PLASTIC FLØW
E33=0, PLANE STRAIN FLØW
APPRØXIMATE FUNCTIØNAL FØRM
NUMERICAL CALCULATIØNS
T(EQV)
0.00
0.20
0.40
0.60
0.80
1.00
0.00
0.50
1.00
1.50
2.00
2.50
3.00
3.50
4.00
0.5*(T11+T22)
F=0.300
F=0.200
F=0.100
F=0.050
F=0.020
F=0.010
F=0.005
F=0.002

FIGURE 5

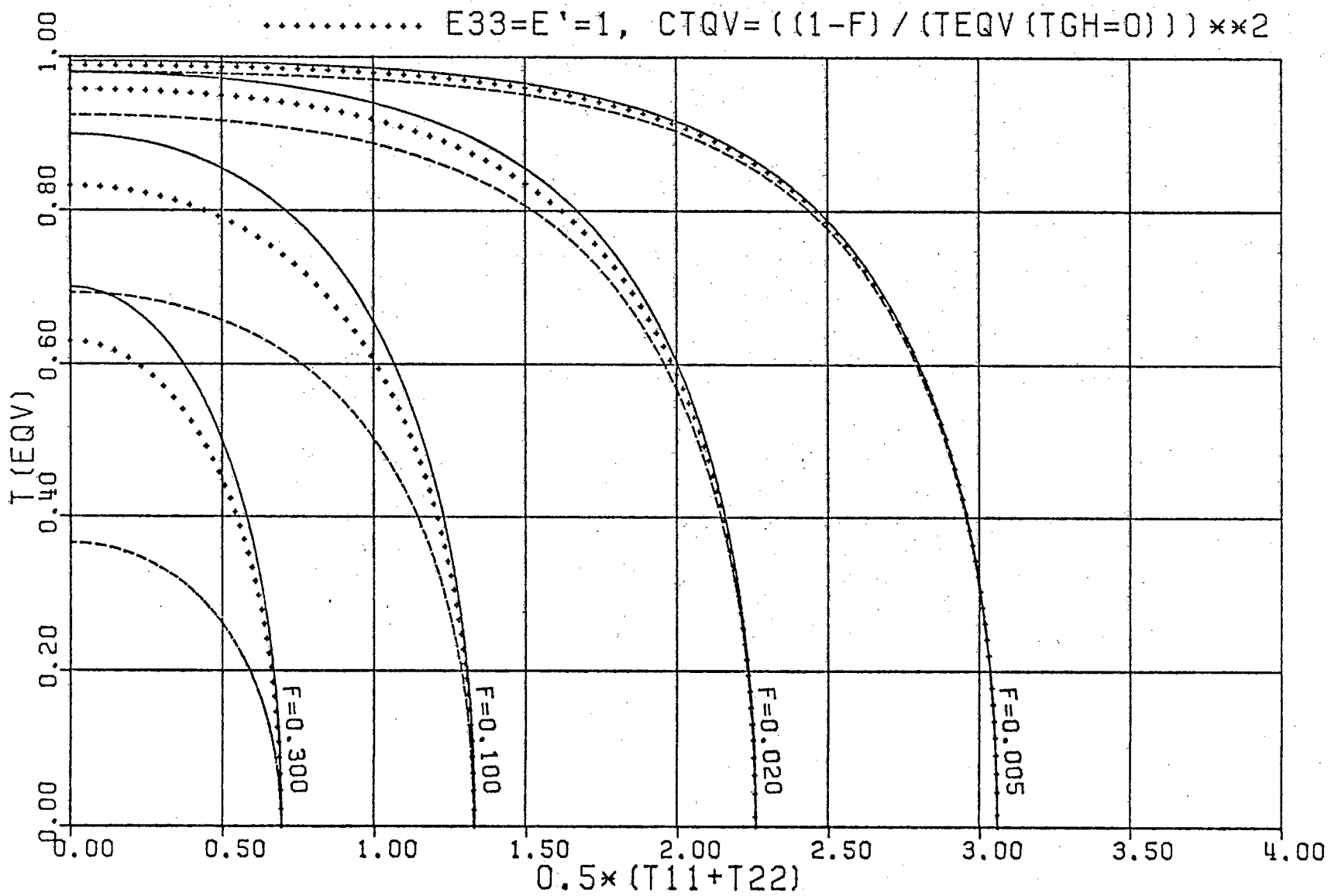
CYLINDRICAL VØIDS, FULLY PLASTIC FLØW
AXISYMMETRIC FLØW
PLANE STRAIN FLØW
E33=E'=1, CTQV=((1-F)/(TEQV(TGH=0)))**2
T(EQV)
0.00
0.20
0.40
0.60
0.80
1.00
0.00
0.50
1.00
1.50
2.00
2.50
3.00
3.50
4.00
0.5*(T11+T22)
F=0.300
F=0.100
F=0.020
F=0.005

FIGURE 6

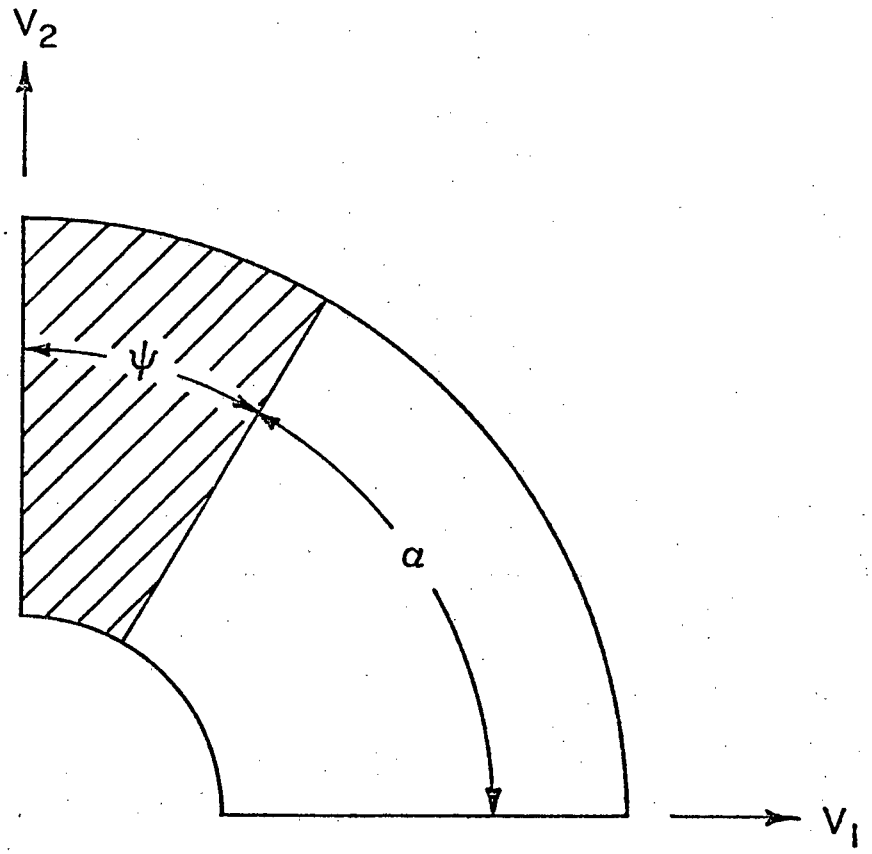

CYLINDRICAL MODEL, RIGID WEDGE
PLANE STRAIN FLOW
QUARTER SECTION

FIGURE 7

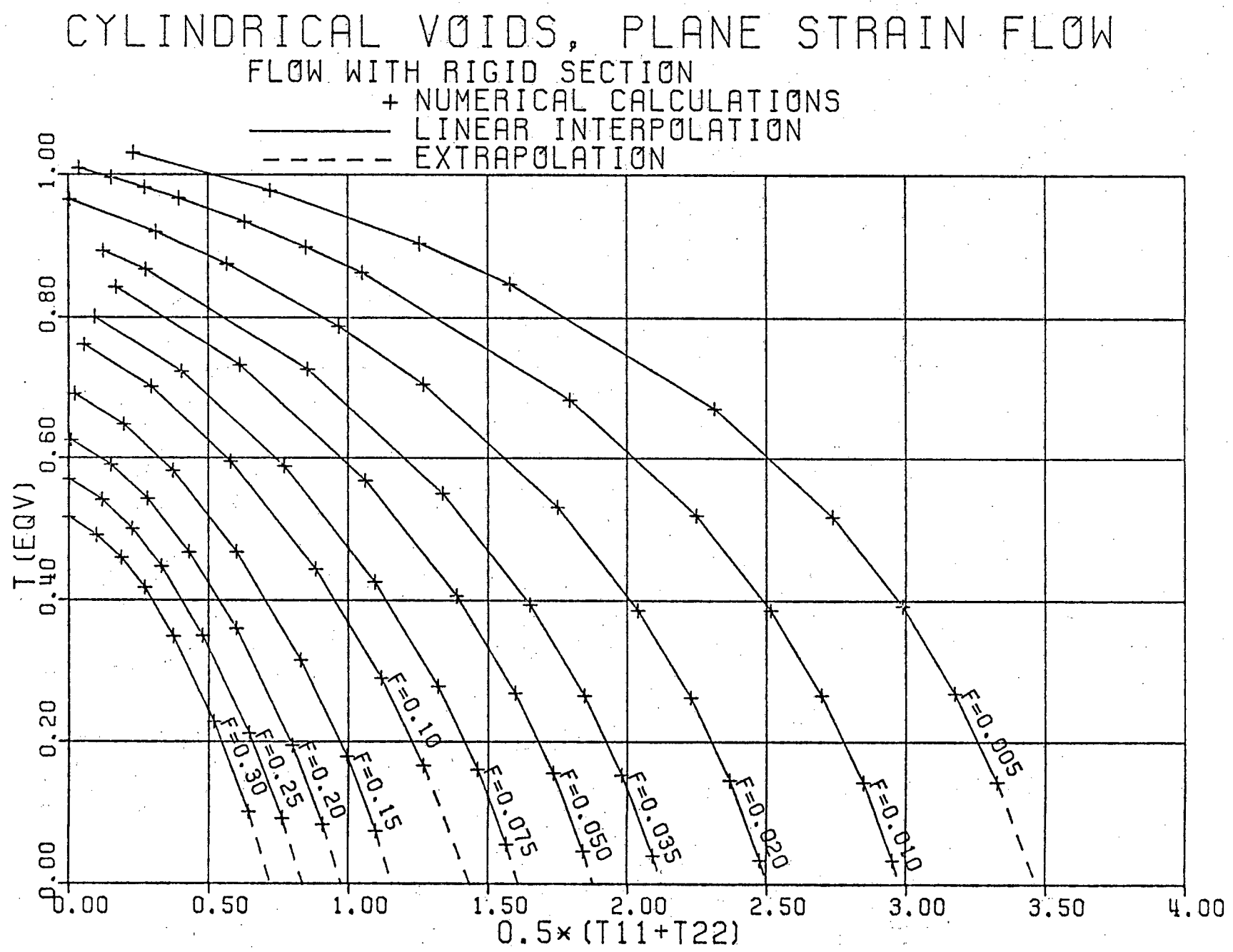
CYLINDRICAL VØIDS, PLANE STRAIN FLØW
FLØW WITH RIGID SECTIØN
+ NUMERICAL CALCULATIØNS
LINEAR INTERPØLATIØN
EXTRAPØLATIØN
T (EQV)
0.00
0.20
0.40
0.60
0.80
1.00
0.00
0.50
1.00
1.50
2.00
2.50
3.00
3.50
4.00
0.5×(T11+T22)
F=0.005
F=0.010
F=0.020
F=0.035
F=0.050
F=0.075
F=0.10
F=0.15
F=0.20
F=0.25
F=0.30

FIGURE 8A

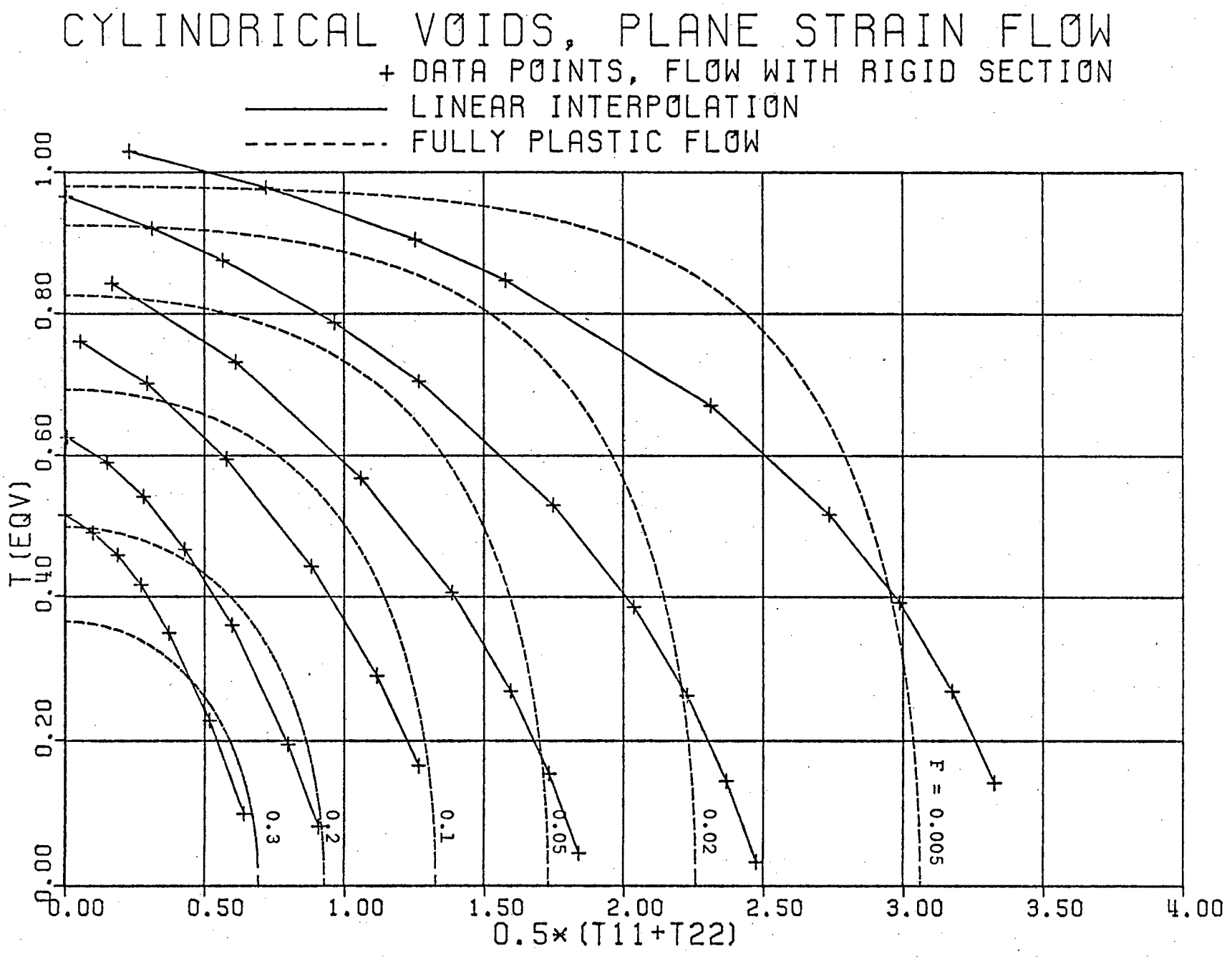
CYLINDRICAL VØIDS, PLANE STRAIN FLØW
+ DATA PØINTS, FLØW WITH RIGID SECTIØN
LINEAR INTERPØLATIØN
FULLY PLASTIC FLØW
T(EQV)
0.00
0.20
0.40
0.60
0.80
1.00
0.00
0.50
1.00
1.50
2.00
2.50
3.00
3.50
4.00
0.5*(T11+T22)
F = 0.005
0.02
0.05
0.1
0.2
0.3

FIGURE 8B

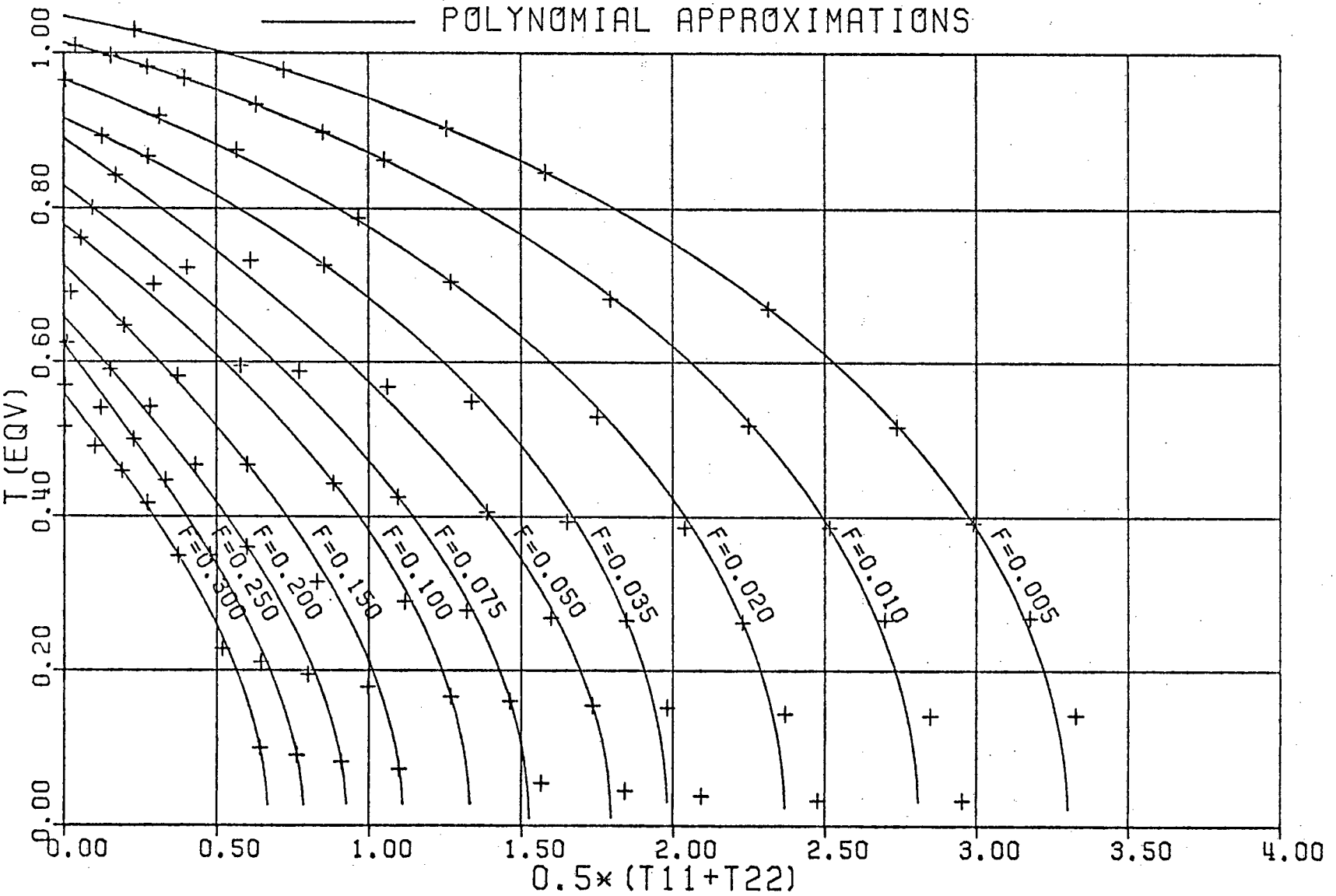
CYLINDRICAL VØIDS, PLANE STRAIN FLØW
FLØW WITH RIGID SECTIØN
+ NUMERICAL CALCULATIØNS
——— PØLYNØMIAL APPRØXIMATIØNS
T (EQV)
0.00
0.20
0.40
0.60
0.80
1.00
0.00
0.50
1.00
1.50
2.00
2.50
3.00
3.50
4.00
0.5* (T11+T22)
F=0.300
F=0.250
F=0.200
F=0.150
F=0.100
F=0.075
F=0.050
F=0.035
F=0.020
F=0.010
F=0.005

FIGURE 9A

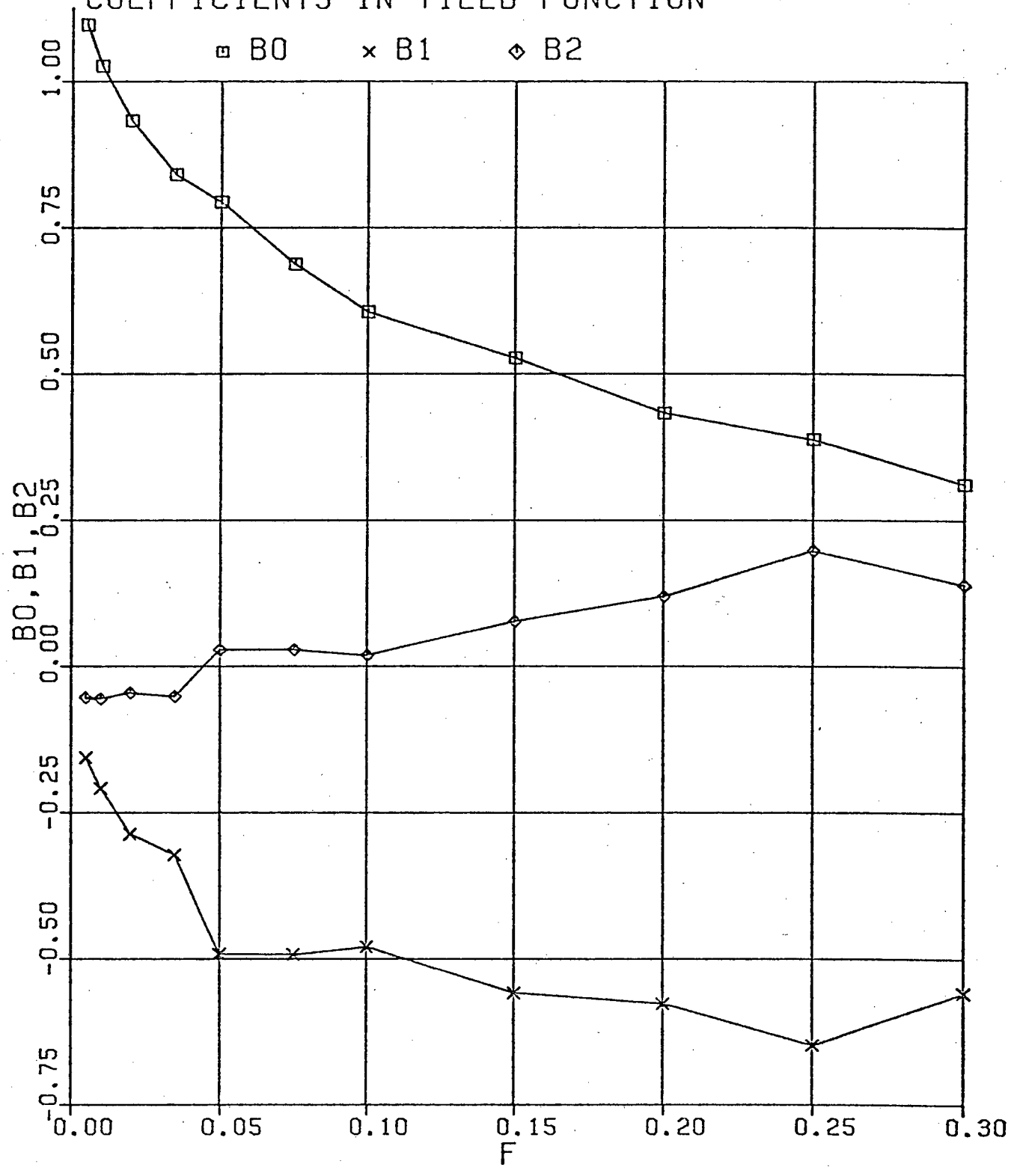
CYLINDRICAL VØIDS, PLANE STRAIN
FLØW WITH RIGID SECTIØN
CØEFFICIENTS IN YIELD FUNCTIØN
B0
B1
B2
1.00
0.75
0.50
0.25
0.00
-0.25
-0.50
-0.75
B0, B1, B2
0.00
0.05
0.10
0.15
0.20
0.25
0.30
F

FIGURE 9B

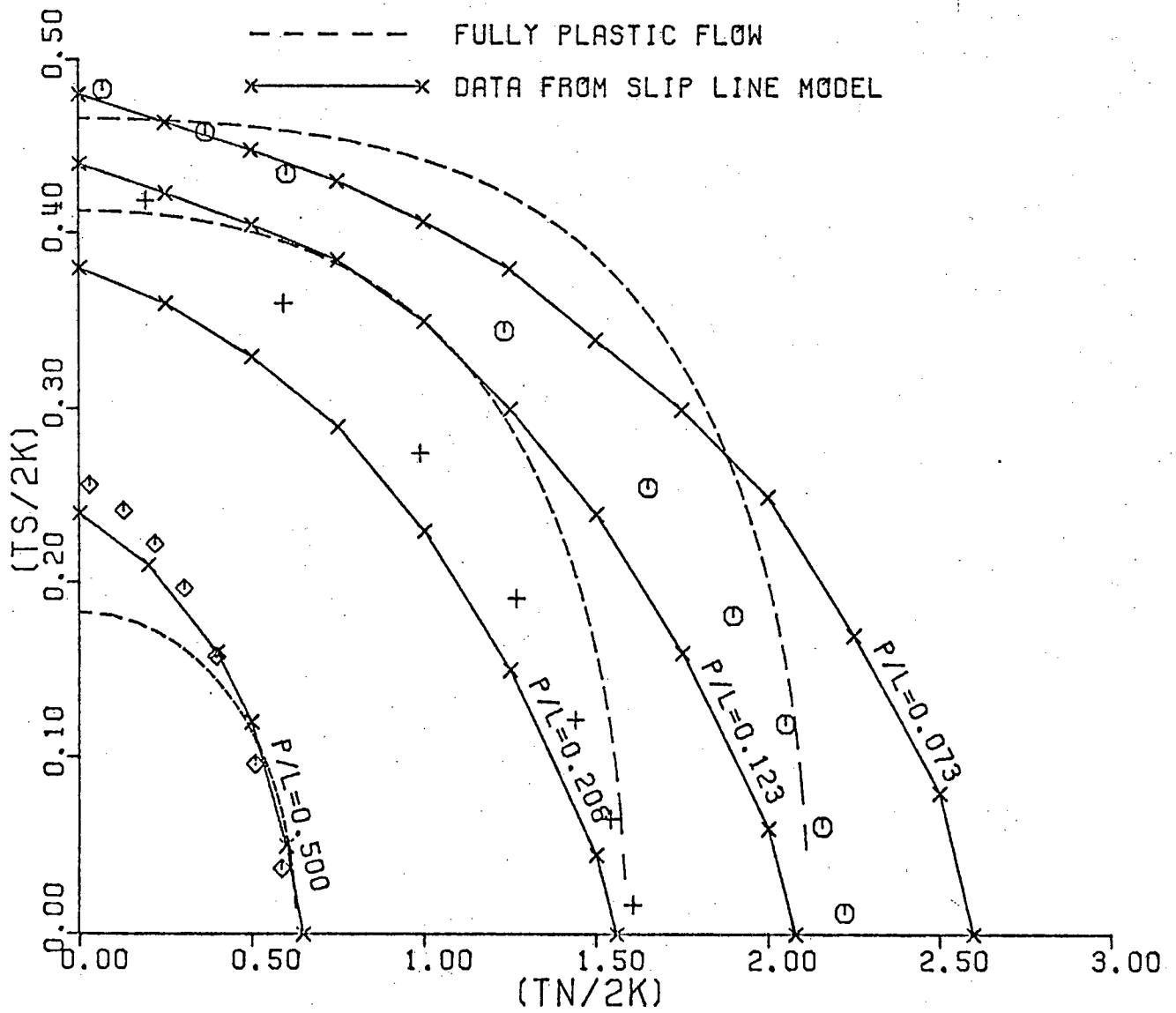
CYLINDRICAL VØIDS, PLANE STRAIN FLØW
COMPARISØN ØF WEDGE DATA TØ SLIP LINE MØDEL
RIGID WEDGE
F=0.0178
F=0.05
F=0.30
FULLY PLASTIC FLØW
DATA FRØM SLIP LINE MØDEL
P/L=0.073
P/L=0.123
P/L=0.208
P/L=0.500
(TS/2K)
(TN/2K)
0.00
0.10
0.20
0.30
0.40
0.50
0.00
0.50
1.00
1.50
2.00
2.50
3.00

FIGURE 10

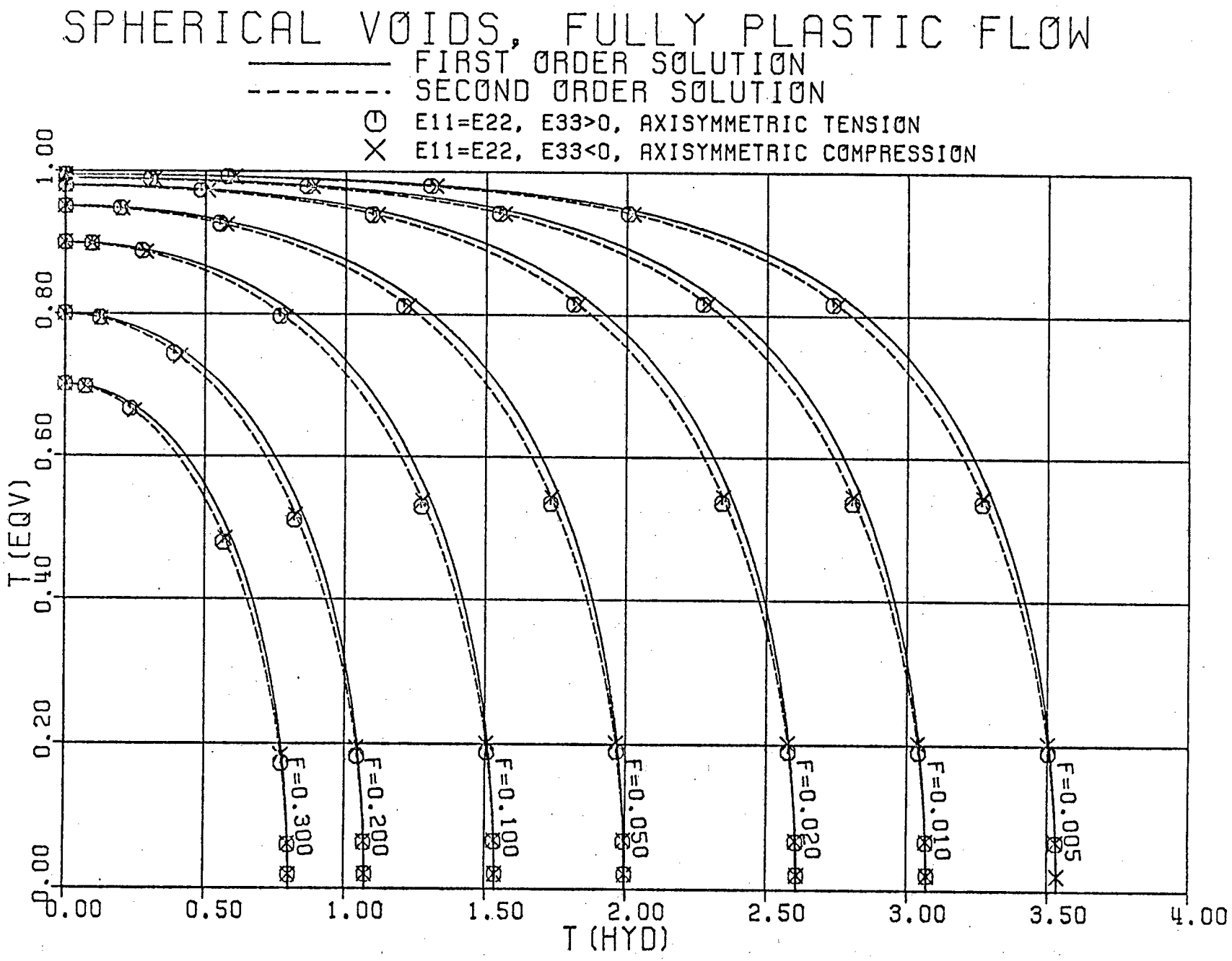
SPHERICAL VØIDS, FULLY PLASTIC FLØW
FIRST ØRDER SØLUTIØN
SECØND ØRDER SØLUTIØN
E11=E22, E33>0, AXISYMMETRIC TENSIØN
E11=E22, E33<0, AXISYMMETRIC CØMPRESSIØN
T (EQV)
T (HYD)
0.00
0.20
0.40
0.60
0.80
1.00
0.00
0.50
1.00
1.50
2.00
2.50
3.00
3.50
4.00
F=0.300
F=0.200
F=0.100
F=0.050
F=0.020
F=0.010
F=0.005

FIGURE 11

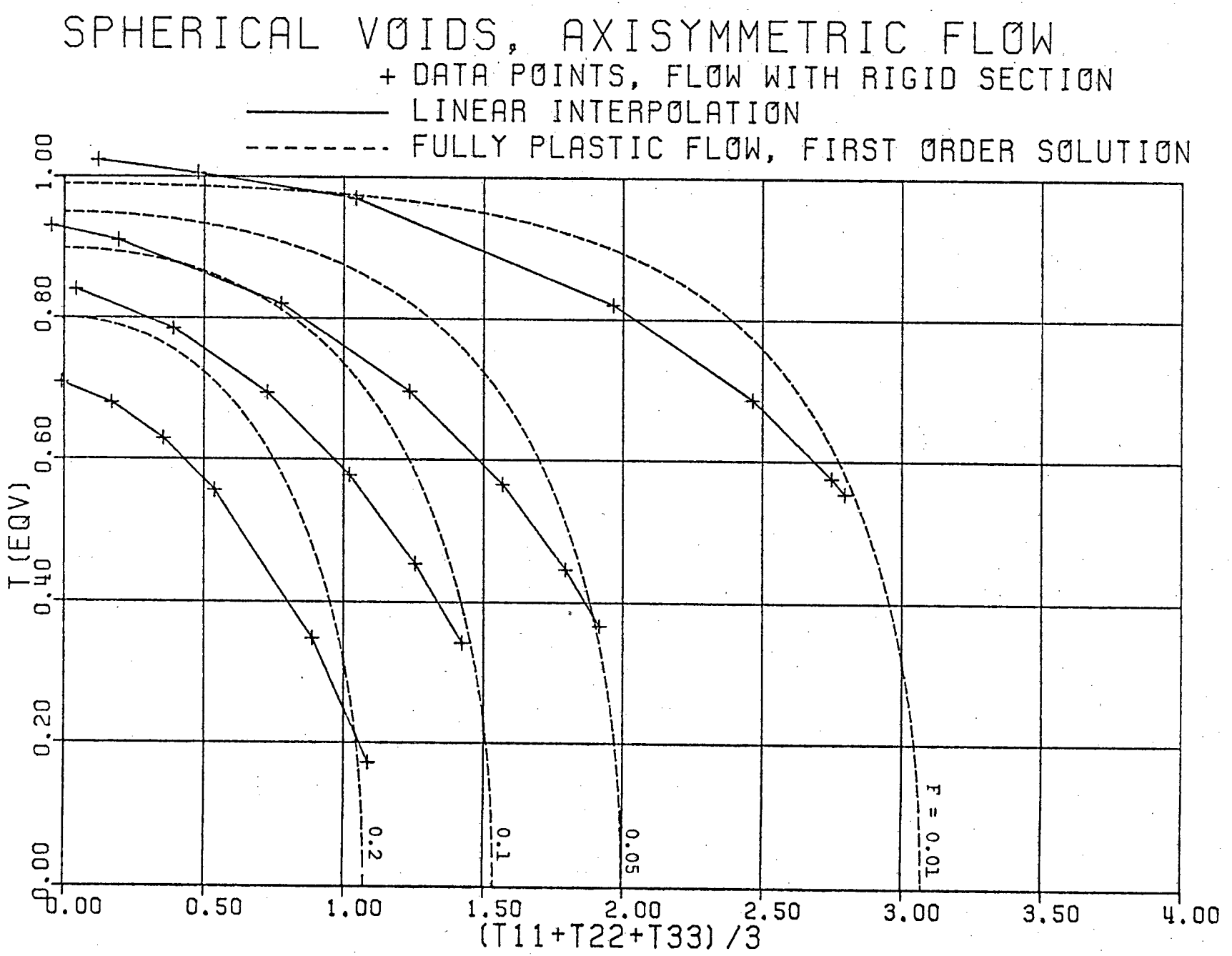
SPHERICAL VØIDS, AXISYMMETRIC FLØW
+ DATA PØINTS, FLØW WITH RIGID SECTIØN
LINEAR INTERPØLATIØN
FULLY PLASTIC FLØW, FIRST ØRDER SØLUTIØN
T (EQV)
0.00
0.20
0.40
0.60
0.80
1.00
0.00
0.50
1.00
1.50
2.00
2.50
3.00
3.50
4.00
(T11+T22+T33) /3
F = 0.2
F = 0.1
F = 0.05
F = 0.01

FIGURE 12

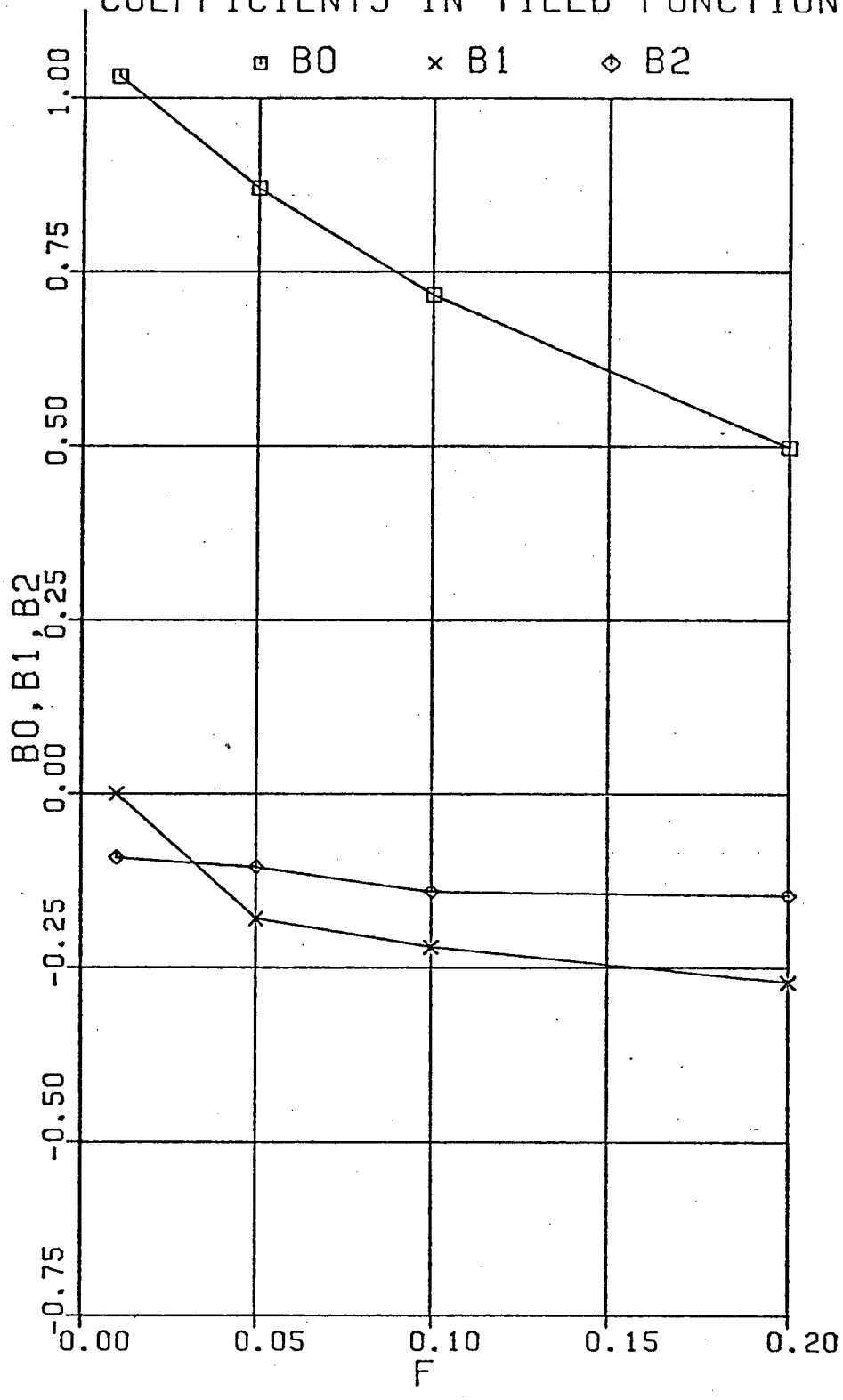
SPHERICAL VØID MØDEL
FLØW WITH RIGID SECTIØN
CØEFFICIENTS IN YIELD FUNCTIØN
B0
B1
B2
1.00
0.75
0.50
0.25
0.00
-0.25
-0.50
-0.75
B0, B1, B2
0.00
0.05
0.10
0.15
0.20
F

FIGURE 13

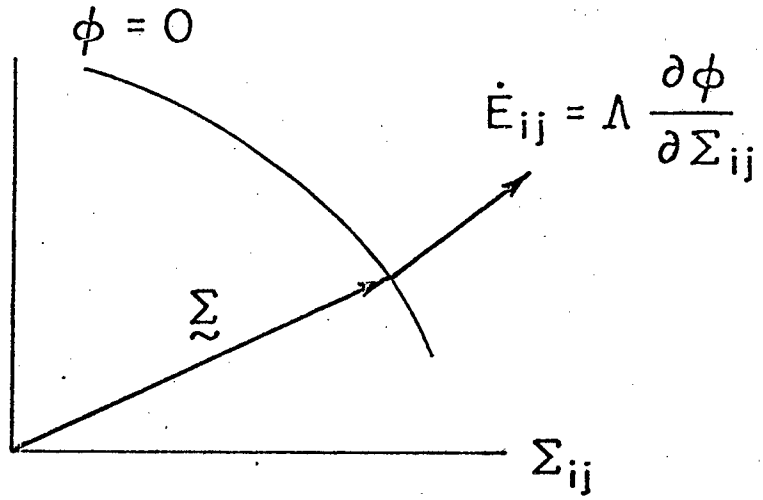

FIGURE 14A

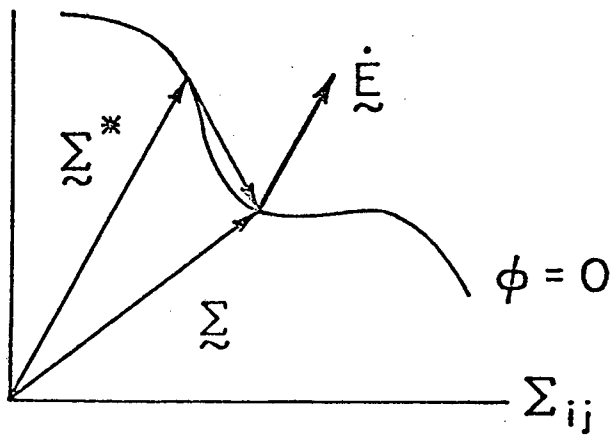

FIGURE 14B